Structural lateral dynamic stability requirements due to pedestrian loading

Bronisław Czaplewski

bronislaw.czaplewski@pwr.edu.pl

Wrocław University of Science and Technology https://orcid.org/0000-0001-7775-8993

Mateusz Bocian

Wrocław University of Science and Technology, University of Leeds https://orcid.org/0000-0002-3539-5474

Research Article

Keywords: bridge design, pedestrian-structure interaction, vibration serviceability, probabilistic stability criteria, London Millennium Bridge, Clifton Suspension Bridge, Squibb Park Bridge

Posted Date: July 22nd, 2025

DOI: https://doi.org/10.21203/rs.3.rs-7162734/v1

Additional Declarations: The authors declare no competing interests.

Structural lateral dynamic stability requirements due to pedestrian loading

Bronisław Czaplewski[1,*] and Mateusz Bocian[1,2]

[1] *Faculty of Civil Engineering, Wrocław University of Science and Technology, Wrocław, Poland*
[2] *School of Civil Engineering, University of Leeds, Leeds, UK*
[*] *Corresponding author: bronislaw.czaplewski@pwr.edu.pl*

Abstract

The inverted pendulum pedestrian model (IPM) for walking on laterally-oscillating structures, originally proposed by Macdonald [1], has been recently calibrated using data from pedestrians walking on a laterally-oscillating instrumented treadmill and generalised for predictive use in Czaplewski et al. [2]. The former task was accomplished by defining an empirically-derived foot placement control law. The latter task was accomplished by relating the parameters of this law to the basic anthropometric and gait characteristics of the pedestrian. Closed-form solutions for the long-term average lateral forces obtained from the generalised IPM were then derived in Czaplewski & Bocian [3] based on the framework introduced by McRobie [4]. These solutions were used to obtain the probabilistic lateral dynamic (in)stability criteria for structures subjected to pedestrian loading presented in this paper. A framework introduced in Bocian et al. [5] is used in which stability requirements are expressed in terms of the pedestrian Scruton number and the critical number of pedestrians. To achieve this goal it was necessary to propose a framework for defining a statistical model of the anthropometric parameters used within the IPM solutions, relevant for a given population of pedestrians. It was also necessary to define IPM validity criteria enabling spurious solutions to be omitted from the analysis. To make the proposed structural stability criteria applicable in engineering practice, a framework had to be defined enabling simplified envelopes of the self-excited forces to be obtained. Crucially, these simplified envelopes should not penalise structural solutions, rendering them overly conservative. The proposed stability criteria are evaluated based on two case studies of bridges prone to pedestrian-induced lateral dynamic instability. The relatively recent occurrence of instability on the Squibb Park Bridge and its consequences are presented here in detail, as this case is currently little known in the structural engineering community.

Keywords: bridge design, pedestrian-structure interaction, vibration serviceability, probabilistic stability criteria, London Millennium Bridge, Clifton Suspension Bridge, Squibb Park Bridge

1 Introduction

Significant advances in understanding of pedestrian lateral loading on structures have been made in the years following the instability of the London Millennium Footbridge (LMF) on its opening day [6]. The evidence for the dominant role of pedestrian-structure interaction mechanism in causing structural instability was obtained from measurements on full-scale bridges [7], [8], [9], [10], [11], [12], [13] and purpose-built experimental platforms [2], [14], [15], [16], [17], [18], [19], [20], [21], [22]. Numerous modelling approaches have been proposed to capture pedestrian behaviour on laterally-oscillating structures with varying level of success [16], [23], [24], [25], [26], [27], [28], [29], [30], [31], [32].

Despite these advances in knowledge, the design of structures, particularly bridges, against pedestrian-induced lateral instability remains a high-risk activity. This is because structural codes development generally lags the challenges of engineering practice. Perhaps the best recent illustration of this is the protracted

litigation that followed the failed retrofit of the Squibb Park Bridge (SPB) in the USA which suffered from excessive pedestrian-induced vibrations. The case against the SPB's designer ended in a no-liability settlement, thanks to which the SPB owner recovered $1.95M. Whatever the verdict, both parties involved in this project and the people the SPB was to serve cannot call themselves the winners.

It seems the 2nd generation of Eurocodes, which is currently under development, will not address this problem. The considered proposal is to effectively adopt the provisions reported from two European research projects funded through the Research Fund for Coal and Steel (RFCS), namely SYNPEX [33], i.e. Advanced Load Models for Synchronous Pedestrian Excitation and Optimised Design Guidelines for Steel Footbridges, and HIVOSS [34], i.e. Human Induced Vibrations of Steel Structures, which concluded more than 15 years ago. These provisions rely on harmonic load models in which pedestrian-structure interaction is not inherently captured. However, synchronisation of pedestrian footsteps to the lateral structural motion is intrinsically considered, which is known not to be the dominant structural excitation mechanism [16], [19], [20], [21]. Therefore, their applicability is, at best, uncertain. Perhaps this is the reason for these provisions to be included within the 2nd generation of Eurocodes in the form of an informative annex. This is to say that they can be used should a national annex be unavailable.

In many countries which adopted Eurocodes, there is still no national annex regulating the design of structures against pedestrian-induced loading. From these in which there is, arguably the most advanced design guidelines against pedestrian-induced lateral loading are included in the British National Annex to Eurocode 1 [35]. This is a consequence of the significant effort spent on solving this problem in the wake of the lateral instability observed on the LMF [6]. These design guidelines originate from a loading model accounting for the legged nature of human locomotion [36] – which was a notable breakthrough from the harmonic models of pedestrian loading – in which synchronisation of pedestrian gait to the lateral structural motion is not a necessary condition for the occurrence of structural instability. However, at their culmination, these guidelines are adjusted to match the results of limited measurements from the LMF only. Therefore, their universal applicability remains uncertain.

The design of structures is inherently associated with risk management. To facilitate this task in the context of lateral structural stability, it is postulated that the relevant design guidelines should meet the following requirements:

(i) *They should be derived from first principles.* Given the developments in our understanding of pedestrian-structure interaction over the last two decades, there is no reason why the design guidelines should be phenomenological. Phenomenological guidelines are those containing design provisions that attempt to link cause and effect either without necessarily considering the underlying mechanisms or adopting uncertain assumptions. This is typical of the early stages of the development of theory describing observations. In the context considered, the quintessential example of this are the pedestrian loading models based on the preferential-phase synchronisation of the timing of pedestrian footsteps to the lateral structural motion – a condition known as *synchronous lateral excitation* or *lock-in* [6], [37]. This condition is now known to be neither the dominant structural excitation mechanism nor even necessary for structural instability to occur [16], [18], [19], [20]. To address this shortcoming, design guidelines should be based on a pedestrian model that captures the fundamental relationships between pedestrian anthropometric and gait characteristics, and bridge dynamics. This will ensure that the mechanisms governing the observed behaviours are understood and taken into account.

(ii) *They should be indiscriminate.* Pedestrian-induced lateral structural instability has been observed on bridges varying in size, principal load bearing mechanism, construction materials and location – see Tables 1 and 2 in [38]. What unifies all those instability cases is the structural excitation mechanism. Therefore, there is an argument to be made for the design guidelines to be universal. This is to say that they should be generally applicable for any given structure and any given population of pedestrians.

(iii) *They should be specific, but not restrictive.* This means that they should give the designer the confidence to make informed choices whilst accounting for the specific structural characteristics and operational conditions which may differ from project to project. The structural characteristics include the dynamic properties such as the modal frequency, mass, damping and mode shape, and the dimensions. The operational conditions may relate to the specific population of users, their number and distribution on the structure. All these factors can determine the critical loading conditions.

(iv) *They should be adaptable.* The target service life for bridges during which they are expected to remain operational may vary depending on their role and importance. Nevertheless, footbridges and road bridges have been known to suffer from pedestrian-induced lateral instability. A good example of the latter class is the Auckland Harbour Bridge (AHB) in New Zealand [39]. This large bridge repeatedly experienced excessive lateral vibrations when occupied by crowds of walking pedestrians. This occurred during Maōri land marches of 1975 and 2004, and most recently in 2022 during demonstrations against COVID-19 vaccine mandate. The AHB, inaugurated in 1954, was never envisaged to experience the rapidly increasing level of traffic. It was widened as soon as in 1969 by the addition of two lanes on each side, cantilevered from the piers. These lanes are currently dedicated to road traffic, but on the rare occasions pedestrian traffic is allowed, they can suffer from the excessive lateral response.

Modern bridges are required to withstand many decades of use. Eurocode 0 (BS EN 1990:2002+A1:2005) enforces the service life of 100 years [40], which has been extended in the UK to 120 years according to the UK National Annex to Eurocode 1 (NA+A1:2020 to BS EN 1991-2:2003) [35]. AASHTO (American Association of State Highway and Transportation Officials), which is equivalent to the National Highways in the UK, suggests the design service life for steel and concrete highway bridges between 75 and 150 years [41]. Just like the road traffic loading in the case of the AHB, pedestrian loading is likely to change in this long-term perspective. A recent study predicts over half of the global population of adults to be overweight or obese by 2050 [42]. Taking this into consideration, the design guidelines should enable the assessment of instability not only for the current users of structures, but also be capable of taking into account future population trends.

(v) *They should be simple enough to be used in engineering practice.* There is a balance to be struck between detail and clarity. Simpler design guidelines prevent from errors being made but may not capture the expected structural behaviour precisely. They may still be acceptable, provided they do not penalise the design, rendering it overly conservative.

Considering all of the above, the overreaching aim of this study is to define design provisions against lateral dynamic instability for structures subjected to the loading from walking pedestrians. Underpinning the development of these design provisions are the requirements stated in points (i) – (v). The outputs from the calibrated and generalised IPM defined in [2] and [3] are used for this purpose, thus satisfying (i). To improve the generalised IPM accuracy, also purported in (i), an analytical criterion is derived enabling solutions violating the kinematic constraints of human walking gait to be identified and omitted from further processing. The lateral dynamic stability criteria are defined based on thereof validated outputs from the generalised IPM using a framework introduced in [5]. These criteria are expressed in the probabilistic sense, taking into account the structural characteristics and operational conditions, thus satisfying (iii). A statistical model of pedestrian anthropometric parameters is proposed applicable for any given population of pedestrians, thus satisfying (ii). The outputs from this model are used to determine the equivalent added damping and mass for the considered population of pedestrians for use within the probabilistic stability criteria, thus satisfying (iv). An algorithm is also proposed enabling piecewise-linear envelopes of the critical equivalent added damping and its standard deviation to be defined. This makes the proposed probabilistic stability criteria suitable for the inclusion in codified design guidelines, thus satisfying (v).

The rest of the paper is organised as follows. Section 2 presents research materials and methods. The generalised IPM is presented in Section 2.1, closed-form long-term solutions of the lateral self-excited forces

derived from the generalised IPM are presented in Section 2.2, and probabilistic stability criteria are presented in Section 2.3. The results of this study are presented and discussed in Section 3. The anthropometric data for populations of selected European countries and the USA are presented in Section 3.1. The statistical model of of the anthropometric parameters from which inputs to the generalised IPM can be obtained is presented in Section 3.2. The analytical criterion enabling solutions of the generalised IPM violating kinematic gait constraints to be identified is derived in Section 3.3. The self-excited forces expressed in terms of the equivalent added damping and mass are established for an exemplar population in Section 3.4. The added mass effect, which can shift the stability boundaries, is established in Section 3.4.1, and the critical equivalent added damping and its standard deviation is established in Section 3.4.2. The algorithm enabling piecewise-linear envelopes of the critical equivalent added damping and its standard deviation to be obtained is presented in Section 3.4.3. Two case studies conducted to evaluate the proposed lateral dynamic stability criteria are presented in Section 3.5. The concluding remarks are presented in Section 4.

2 Materials and methods

This section presents the main components necessary to define provisions against structural lateral dynamic instability. The calibrated and generalised IPM, as proposed in Czaplewski et al. [2], is presented in Section 2.1. The closed-form solutions for the long-term average self-excited forces obtained from the generalised IPM, as derived in Czaplewski & Bocian [3], are presented in Section 2.2. The probabilistic stability criteria, as derived in Bocian et al. [5], are presented in Section 2.3.

2.1 Generalised inverted pendulum pedestrian model (IPM)

The long-term structural dynamic stability of the considered mode under the action of pedestrians is mainly affected by the component of force applied at the modal frequency, f_b [4], [5]. That force component is captured by the generalised IPM, as shown in Czaplewski et al. [2]. Assuming that the mode behaves linearly, the equation of motion for that mode can be defined by [5]:

$$\left[M + \sum_{i=1}^{N} \Delta M_i \left(\omega_b\right) \phi_i^2\right] \ddot{X} + \left[C + \sum_{i=1}^{N} \Delta C_i \left(\omega_b\right) \phi_i^2\right] \dot{X} + KX = F_{\mathrm{rem}} \tag{1}$$

where M, C and K are the modal mass, damping and stiffness, respectively, N is the number of pedestrians on the structure, ΔC_i and ΔM_i are the equivalent added damping and mass, respectively, for the i-th pedestrian, which are dependent on the structural vibration frequency, $f_b = \frac{\omega_b}{2\pi}$, ϕ_i is the modal amplitude at the location of i-th pedestrian, X is the generalised displacement with dots over symbols representing relative differentiation with respect to time, and F_{rem} contains all remaining components of pedestrian lateral force, i.e. it does not include the self-excited forces at f_b. All components of F_{rem} either provide background excitation to the structure, since they are detuned from f_b, or their magnitudes are too small to cause any significant long-term effects [1]. Therefore, in the analysis of structural stability those components can be discarded by setting $F_{\mathrm{rem}} = 0$.

The generalised IPM, presented in Czaplewski et al. [2], is the calibrated and parametrised IPM originally proposed by Macdonald in [1], which was inspired by the work of Barker [36]. It consists of a mass, m, equivalent to the pedestrian mass and concentrated at a point referred to as the centre of mass (CoM), sitting on top of a massless rigid leg of the length l. The IPM is a two-dimensional model confined to the frontal plane, i.e. a vertical plane perpendicular to the direction of progression. It represents pedestrian body dynamics during the single-support phase of gait, in which only one leg is in contact with the ground. The double-support phase of gait, in which the support of the body is transferred from one leg to the other, is omitted, hence the switch between steps is instantaneous while preserving the lateral velocity of the CoM.

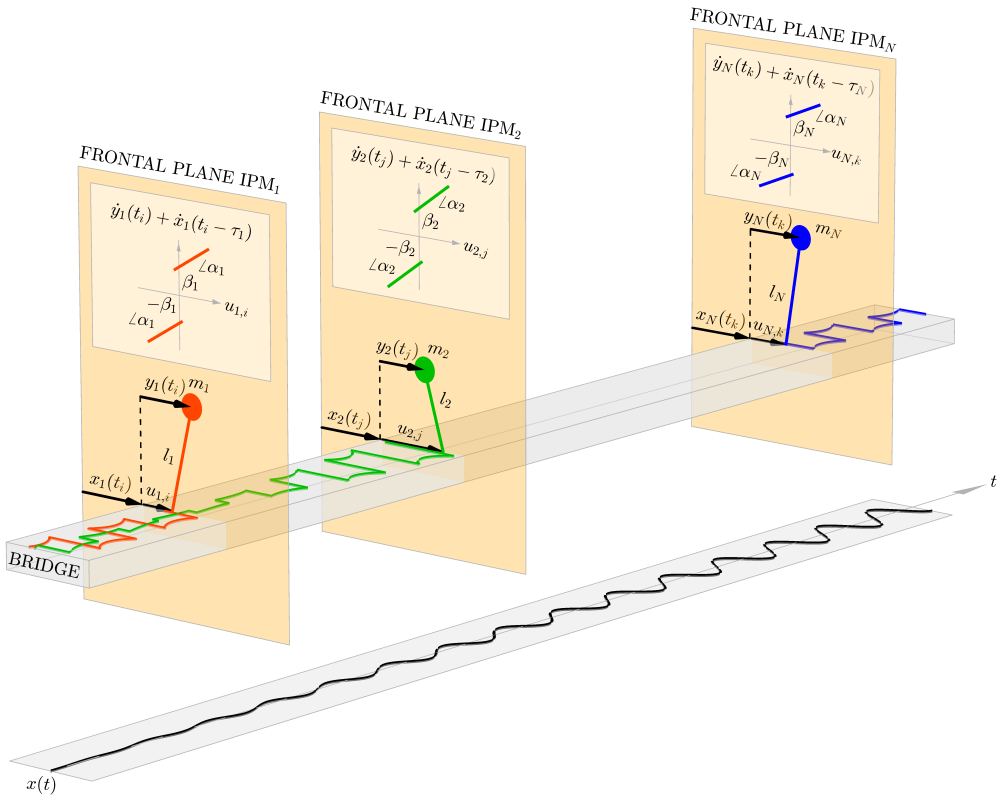

Figure 1: Diagrammatic representation of a structure during the development of lateral instability due to the loading from N inhomogeneous pedestrians represented by the generalised inverted pendulum pedestrian models (IPMs).

To ensure that balance is maintained, a foot placement control law of the type proposed by Hof et al. [43] is implemented within the generalised IPM. The position of the centre of pressure (CoP), which is effectively the origin of the ground reaction force vector, that being equivalent and opposite to the vector of the force exerted by the pedestrian onto the structure, at the initiation of the step is adjusted according to:

$$u_{i,j} = y_i\left(t_{i,j}\right) + \alpha_i\left[\dot{x}_i\left(t_{i,j} - \tau_i\right) + \dot{y}_i\left(t_{i,j}\right)\right] \pm \beta_i \tag{2}$$

where the subscripts i and j denote quantities defined for the i-th pedestrian and j-th step, respectively, y is the lateral displacement of the CoM relative to an arbitrary point on the structure, x is the lateral displacement of the structure at the location of the i-th pedestrian relative to a stationary (in the absolute sense) reference point, α is the constant of proportionality (i.e. slope), β is the constant offset (i.e. intercept) which is taken as positive and negative for steps taken with the right and left leg, respectively, $t_{i,j}$ is the time instance of the initiation of the j-th step by the i-th pedestrian, τ is the time offset, and dots over symbols represent relative derivatives with respect to time t.

The foot placement control law in Eq. 2 differs from the law proposed by Hof et al. [43], adopted in the original IPM proposed by Macdonald [1], in that coefficients α and β in Eq. 2 are empirically obtained constants generalised based on the pedestrian anthropometric characteristics. Therefore, α corresponds to $1/\Omega_p$ in Hof et al. [43], where Ω_p is the angular pendulum frequency defined as $\sqrt{g/l}$ where g is the gravitational acceleration and $l = 1.34L$, where L is the pedestrian leg length, and β corresponds to the constant lateral offset termed the margin of stability, denoted b_{min} in Hof et al. [43]. Furthermore, the time offset τ introduced in Eq. 2, but missing in Hof et al. [43], accounts for the omission of the double-

support phase of gait within the IPM and neuromotor control, i.e. issues related to the integration of sensory information and the execution of motor activities enabling the pedestrian to remain balanced. Both these issues are discussed in more detail in Section 3.1.4 in Czaplewski et al. [2].

The anthropometric characteristics defining α and β are the pedestrian height, H, leg length taken as the distance between the lateral malleous and the top of greater trochanter, L, pelvis width taken as the lateral distance between the points on the two sides of pedestrian body marking the top of greater trochanter, P and shoulder width taken as the lateral distance between points on the two sides of pedestrian body marking the glenohumeral axes, S, such that:

$$\alpha_i = 0.501\sqrt{H_i} - 1.462\sqrt{\frac{L_i}{H_i}} + 1.3\sqrt{\frac{P_i}{H_i}} + 1.747\sqrt{\frac{S_i}{H_i}} - 0.808 \tag{3}$$

$$\beta_i = 0.0752\alpha_i + \mathcal{N}(-0.0106,\, 0.0015) \tag{4}$$

where $\mathcal{N}(\mu,\, \sigma)$ is a random variable drawn from normal distribution with mean μ and standard deviation σ. The time offset, τ, is defined in terms of the stride frequency, f_s:

$$\tau_i = -0.0116 f_{s,i}^{1.571} + 0.0476 f_{s,i}^{-1} \tag{5}$$

The CoM equation of motion, assuming the leg remains close to vertical during walking, is given by:

$$\ddot{y}_i\left(t\right) + \frac{1}{\alpha_i^2}\left[u_{i,j} - y_i\left(t\right)\right] = -\ddot{x}\left(t\right) \tag{6}$$

and the total lateral force from the pedestrian onto the structure is given by:

$$F_i\left(t\right) = -m_i\left[\ddot{x}\left(t\right) + \ddot{y}_i\left(t\right)\right] = \frac{m_i}{\alpha_i^2}\left[u_{i,j} - y_i\left(t\right)\right] \tag{7}$$

The pedestrian-specific parameters, i.e. mass, m_i, together with α_i, β_i and τ_i defined in Eqs. 3, 4 and 5, respectively, determine the long-term average self-excited forces at the modal frequency, ΔC_i and ΔM_i, which are used in the generalised equation of motion in Eq. 1. These forces are defined in Section 2.2.

2.2 Closed-form solutions of the long-term average self-excited forces

The closed-form solutions for the long-term average lateral forces generated from the generalised IPM at the structural oscillation frequency were derived in Czaplewski & Bocian [3] based on the formulation of the original IPM porposed by Macdonald [1] introduced by McRobie [4]. Those solutions cover two types of pedestrian stepping behaviour on laterally-oscillating structures: phase drift and synchronisation. Phase drift occurs when pedestrian stride frequency is constant and different from the structural oscillation frequency, hence the phase between the pedestrian and structural motion evolves at a constant rate. Synchronisation occurs when those two frequencies are exactly the same, hence the phase between the pedestrian and structural motion is constant. However, they do not cover phase pulling, i.e. the case when the pedestrian stride frequency is modulated by the structural motion, hence the phase between the pedestrian and structural motion evolves at a varying rate. Whether all these cases should be taken into account in defining the structural lateral dynamic stability criteria is still an issue of debate.

Phase pulling mechanism was first discovered from the analysis of pedestrian-structure interaction on vertically-oscillating structures using an inverted pendulum pedestrian model in Bocian et al. [44], [45]

and some empirical evidence for this was provided in Nessler et al. [46]. It was advocated by McRobie et al. [47] that the same mechanism, albeit termed intermittency and limited to one mode of phase modulation only, could explain the underestimation of the negative damping effect arising from pedestrian-structure interaction on laterally-oscillating structures from laboratory measurements relative to that obtained from measurements on full-scale bridges. Empirical evidence supporting this claim was provided from the experimental campaign by Bocian et al. [19], although two modes of phase pulling were identified distinguished based on whether f_s falls below or above f_b, in line with the model predictions [44], [45]. Another explanation was offered in McRobie [4] to reconcile the outputs from the IPM and measurements from the LMF [6] in that a proportion of pedestrians in a crowd could synchronise their gait with the lateral structural motion at phases increasing the detrimental damping effect.

Whether the phase-pulling mechanism and synchronisation should be incorporated in the provisions against structural instability is still unclear. Bocian et al. [19] identified phase pulling in only 5 out of 137 conducted tests with pedestrians walking on a laterally-oscillating instrumented treadmill, although the criterion adopted therein for the classification of this stepping behaviour was quite stringent. The same study reported no evidence of preferential phase frequency entrainment (i.e. lock in), while very few occurrences of synchronisation were reported from observations on full-scale structures [38]. Therefore, while neither phase pulling nor synchronisation can be discounted at this point, it is difficult to argue their central role in causing structural instability. Nevertheless, the IPM lends itself to modifications enabling this mechanism to be captured, as shown in [47], [48], [49].

The parametric analyses of the generalised IPM in the case of phase drift presented in Czaplewski & Bocian [3] suggest that pedestrians can generate the effective negative damping much more detrimental to structural stability than the average estimates obtained from the LMF [6]. Therefore, even without making any assumptions as to the occurrence of phase pulling or synchronisation, they can provide more onerous structural (in)stability criteria than those currently available, e.g. [5], [35], [50], [51].

Taking all of the above into consideration, the structural stability criteria presented in this study are based on the solutions of the self-excited forces for the case of phase drift. It needs to be borne in mind that these solutions also contain the occurrence of synchronisation, however ΔC and ΔM are averaged in this case over all possible phase angles. Therefore, for the general case of phase drift, according to [3], ΔC_i and ΔM_i are defined by:

$$\Delta C_i = -\frac{2m_i A^2}{\alpha_i^2 \omega_b^2 T_i} \left(K_1 a_1 - K_2 a_2\right) \tag{8}$$

$$\Delta M_i = \frac{m_i A}{\alpha_i^2 \omega_b^2} \left[1 - \frac{2A}{\omega_b T_i} \left(K_1 a_2 + K_2 a_1\right)\right] \tag{9}$$

where:

$$\begin{aligned}
A &= 1 - \frac{1}{1 + \alpha_i^2 \omega_b^2} \\
K_1 &= 1 - \frac{\alpha_i \omega_b}{A} \sin \psi_{\tau,i} \\
K_2 &= \alpha_i \omega_b \left(1 - \frac{1}{A} \cos \psi_{\tau,i}\right) \\
a_1 &= 1 - e^{\frac{T_i}{2\alpha_i}} \cos \psi_{s,i} \\
a_2 &= e^{\frac{T_i}{2\alpha_i}} \sin \psi_{s,i}
\end{aligned}$$

and $\psi_{s,i} = \frac{\omega_b T_i}{2}$ defines the phase offset per period of a single step, where $T_i = \frac{1}{f_{s,i}}$ is the duration of the gait

cycle, and $\psi_{\tau,i} = \omega_b \tau_i$ defines the phase offset per time lag. As can be seen in Eqs. 8 and 9, the long-term solutions for the average self-excited forces are independent from β_i included in the foot placement control law in Eq. 2, but they are dependent on α_i and τ_i.

Having defined ΔC_i and ΔM_i for any pedestrian with known anthropometric and gait characteristics, a probabilistic framework is required to account for the distribution of the self-excited forces in the population sample loading a structure. Such a framework is presented in Section 2.3.

2.3 Probabilistic stability criteria

A probabilistic framework defining the structural lateral dynamic stability criteria, suitable for use with the generalised IPM, was presented in Bocian et al. [5]. The structural stability boundary for a given mode was derived based on Eq. 1 by applying Fourier transforms and substituting for the structural angular natural frequency $\omega_n = \sqrt{\frac{K}{M}}$ and the damping ratio $\zeta = \frac{C}{2M\omega_n}$ [52]:

$$-\left[1 + \frac{1}{M}\sum_{i=1}^{N} \Delta M_i\left(\omega_b\right)\phi_i^2\right]\omega_b^2 + \left[2\zeta\omega_n + \frac{1}{M}\sum_{i=1}^{N} \Delta C_i\left(\omega_b\right)\phi_i^2\right]\mathrm{i}\omega_b + \omega_n^2 = 0 \tag{10}$$

where $\mathrm{i} = \sqrt{-1}$. Therefore, on the stability boundary of the pedestrians-structure system the following relationships apply [52], [53]:

$$\omega_n = \omega_b\sqrt{1 + \tilde{\mu}_{\Delta M}\left(\omega_b\right) m_r} \tag{11}$$

$$\zeta = -\frac{\omega_b}{\omega_n}\tilde{\mu}_{\Delta C}\left(\omega_b\right) m_r \tag{12}$$

where $m_r = \frac{M_p}{M}$ is the pedestrians to structure mass ratio in which the modal mass of pedestrians is defined as:

$$M_p = \int_0^{L_s} m_p \phi^2 \, ds \tag{13}$$

where L_s is the length of the structure, m_p is the mass of pedestrians per unit length and s is the distance along the structure. In Eqs. 11 and 12, $\tilde{\mu}_{\Delta C}$ and $\tilde{\mu}_{\Delta M}$ are the mean equivalent added damping and mass, respectively, based on the considered population, normalised such that:

$$\tilde{\mu}_{\Delta C} = \frac{\mu_{\Delta C}}{2\omega_b \mu_m} \tag{14}$$

$$\tilde{\mu}_{\Delta M} = \frac{\mu_{\Delta M}}{\mu_m} \tag{15}$$

where μ_m is the average mass of a pedestrian for the considered population.

By analogy with the classical analysis of flutter instability using flutter derivatives in wind engineering [54], [55], a convenient way of expressing the stability boundary in terms of the pedestrian Scruton number was proposed by McRobie & Morgenthal [14]. Using a similar approach, the pedestrian Scruton number is defined as:

$$D = \zeta\frac{M}{M_p} \tag{16}$$

which is effectively a mass-damping parameter. The same approach was adopted in Newland [53], except that D in Eq. 16 is half of the pedestrian Scruton number defined therein. To avoid structural lateral dynamic instability in the considered vibration mode, D should lie above the stability boundary.

Three loading scenarios were considered in [5], for which the pedestrian Scruton number was defined in a probabilistic sense. To simplify the notation, parameters Φ_n can be introduced defining the n-th power of the mode shape integral:

$$\Phi_n = \int_0^{L_s} \phi^n \, ds \tag{17}$$

which can be evaluated for any mode shape. However, for a mode shape defined by p half sine waves, such that:

$$\phi = \sin \frac{p\pi s}{L_s} \tag{18}$$

based on Eq. 17, $\Phi_2 = \frac{1}{2}$ and $\Phi_4 = \frac{3}{8}$ for any integer p. To account for the variability of pedestrian parameters, the standard deviation of the normalised equivalent added damping is used:

$$\tilde{\sigma}_{\Delta C} = \frac{\sigma_{\Delta C}}{2\omega_b \mu_m} \tag{19}$$

together with the confidence limits drawn from normal distribution, such that z_γ corresponds to the $100\,(1-\gamma)$ percent one-sided upper confidence interval, such that for the 95% confidence limit $z_{\gamma=0.05} = 1.645$ and for the 99% confidence limit $z_{\gamma=0.01} = 2.326$.

For the uniform distribution of pedestrians on the structure:

$$\zeta \frac{M}{M_{p,\mathrm{nom}}} > -\tilde{\mu}_{\Delta C} + z_\gamma \tilde{\sigma}_{\Delta C} \frac{1}{\Phi_2 \sqrt{N}} \sqrt{\Phi_4} \tag{20}$$

where the nominal modal mass of pedestrian, $M_{p,\mathrm{nom}}$, can be taken as:

$$M_{p,\mathrm{nom}} = N \mu_m \Phi_2 \tag{21}$$

Therefore, for a sinusoidal mode shape, Eq. 20 simplifies to:

$$\zeta \frac{M}{M_{p,\mathrm{nom}}} > -\tilde{\mu}_{\Delta C} + z_\gamma \tilde{\sigma}_{\Delta C} \sqrt{\frac{3}{2N}} \tag{22}$$

where:

$$M_{p,\mathrm{nom}} = \frac{N \mu_m}{2} \tag{23}$$

For the random distribution of pedestrians on the structure:

$$\zeta \frac{M}{M_{p,\mathrm{nom}}} > -\tilde{\mu}_{\Delta C} + \frac{z_\gamma}{\Phi_2 \sqrt{N}} \sqrt{\tilde{\sigma}^2_{\Delta C} \Phi_4 + \tilde{\mu}^2_{\Delta C} \left(\Phi_4 - \Phi_2^2\right)} \tag{24}$$

which for a sinusoidal mode shape simplifies to:

$$\zeta \frac{M}{M_{p,\mathrm{nom}}} > -\tilde{\mu}_{\Delta C} + z_\gamma \sqrt{\frac{1}{2N}\left(\tilde{\mu}_{\Delta C}^2 + 3\tilde{\sigma}_{\Delta C}^2\right)} \tag{25}$$

For all pedestrians distributed at the maximum of the mode shape:

$$\zeta \frac{M}{M_{p,\mathrm{nom}}} > \frac{\phi_{\max}^2}{\Phi_2}\left(-\tilde{\mu}_{\Delta C} + z_\gamma \tilde{\sigma}_{\Delta C}\frac{1}{\sqrt{N}}\right) \tag{26}$$

For more details on the derivation of the probabilistic stability criteria the reader is referred to Bocian et al. [5]. The remaining problem is the definition of $\tilde{\mu}_{\Delta C}$, $\tilde{\mu}_{\Delta M}$ and $\tilde{\sigma}_{\Delta C}$ based on closed-form solutions presented in Section 2.2 which, according to the generalised IPM presented in Section 2.1, depend on the considered population of pedestrians and their anthropometric characteristics.

3 Results and discussion

To obtain outputs from the calibrated and generalised IPM based on the closed-form solutions presented in Section 2.2, the pedestrian anthropometric data are required, which are defined in Section 3.1. These data are used to establish statistical models of the pedestrian anthropometric parameters presented in Section 3.2. The validity of the calibrated and generalised IPM is then established in Section 3.3, before defining the critical pedestrian-generated forces in terms of the equivalent added damping, ΔC, and equivalent added mass, ΔM, in Section 3.4. To showcase the applicability of the proposed structural stability criteria, case studies of two bridges susceptible to pedestrian-induced lateral instability are presented in Section 3.5. Since these bridges are located in the UK and the USA, the critical stability criteria are established for the two corresponding populations, and additionally for the population of Poland, although the presented methodology can be applied for any population of pedestrians.

3.1 Anthropometric data

The anthropometric data required to define the probabilistic structural stability criteria based on the outputs of the calibrated and generalised IPM were taken from publications reporting these data for the selected countries in Europe, i.e. Poland and the UK [56], and the USA [57]. The data for the UK and the USA will be used in the case studies of bridges prone to the lateral dynamic instability under the action of pedestrians presented in Section 3.5. The anthropometric datasets reported in [56], [57] are given according to ISO 7250 standard [58] providing a convention for describing the anthropometric measurements. Apart from the stature, which was taken as equivalent to the height, H, and the hip breadth, which was taken as equivalent to the pelvis width, P, the datasets also include the shoulder breadth, which is defined in ISO 7250 standard [58] in a different manner than the shoulder width, S, used in the generalised IPM [2]. To account for this difference, a multiplier of 0.83 was applied to the values from [56], [57] to obtain S.

The remaining parameter to define is the leg length, L. Due to lack of suitable data defining this parameter for the considered populations compatible with the measurement method in [18], [19], L was taken herein to reflect the data from tests on the instrumented treadmill used to calibrate the IPM. The mean value of $\frac{L}{H}$ was 0.45 and the standard deviation was 0.0115, hence these values were adopted in all statistical models.

The pedestrian mass is correlated with the height [59], which is captured by the body mass index (BMI), defined by the ratio $\frac{m}{H^2}$, where m is expressed in kg and H is expressed in m. According to the World Health Organization (WHO) [60], in 2016 the mean BMI for men and women in Poland was 27.4 and 25.9 $\mathrm{kg\,m^{-2}}$, respectively, with the corresponding standard deviation of 3.85 and 4.85 $\mathrm{kg\,m^{-2}}$ [61]. According to

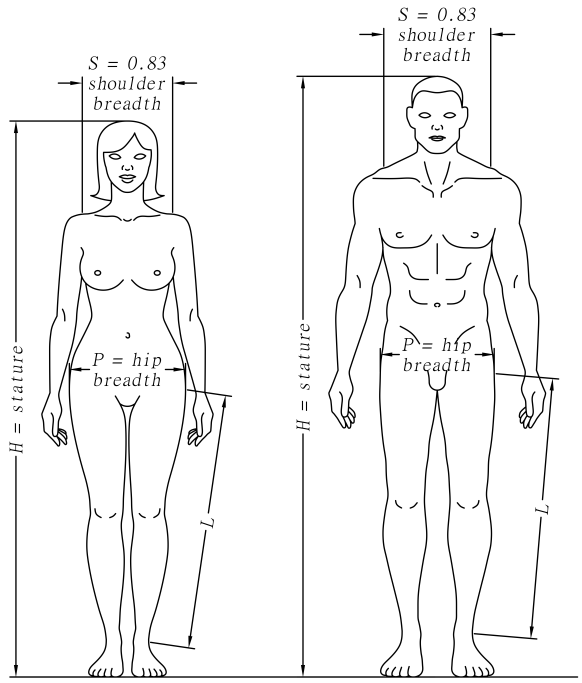

Figure 2: Anthropometric parameters adopted in the calibrated and generalised IPM [2].

Table 1: Anthropometric parameters for the populations of selected countries expressed according to the convention of ISO 7250 [58].

Country	**Gender**	**Stature [m]**			**Hip breadth [m]**			**Shoulder breadth [m]**		
		percentile			**percentile**			**percentile**		
		5th	**50th**	**95th**	**5th**	**50th**	**95th**	**5th**	**50th**	**95th**
Poland	male (48%)	1.660	1.778	1.890	0.311	0.345	0.380	0.376	0.410	0.445
	female (52%)	1.536	1.634	1.740	0.319	0.358	0.388	0.332	0.372	0.416
United Kingdom	male (49%)	1.641	1.775	1.869	0.316	0.363	0.411	0.376	0.412	0.447
	female (51%)	1.514	1.620	1.726	0.332	0.390	0.448	0.338	0.368	0.394
USA	male (49%)	1.648	1.755	1.870	0.308	0.344	0.387	0.384	0.415	0.447
	female (51%)	1.525	1.626	1.740	0.311	0.353	0.400	0.335	0.365	0.396

the British National Health Service (NHS) [62], the mean BMI for men and women in the UK was 27.2 and 26.9 $\mathrm{kg\,m^{-2}}$, respectively, with the corresponding standard deviation of 4.45 and 5.53 $\mathrm{kg\,m^{-2}}$. According to the Vital and Health Statistics [63], which provides official data of the United States Department of Health & Human Services, in 2020 the mean BMI for men and women in the USA was 28.6 and 28.7 $\mathrm{kg\,m^{-2}}$, respectively, with the corresponding standard deviation of 4.63 and 5.63 $\mathrm{kg\,m^{-2}}$.

3.2 Statistical modelling of pedestrian anthropometric parameters

To obtain the mean normalised equivalent added damping and mass defined in Eqs. 14 and 15, respectively, and the standard deviation of the normalised equivalent added damping defined in Eq. 19, it is first necessary to establish a statistical model of the anthropometric parameters representative of the considered population. This procedure involves the following steps, making use of the data in Tables 1 and 2:

(i) Determination of gender based on the binomial distribution.

(ii) Determination of height, H, based on the normal distribution.

Table 2: Anthropometric parameters for the populations of selected countries expressed according to the convention adopted in the calibrated and generalised IPM [2].

Country	**Gender**	**H [m]**	**BMI [kg.m^{-2}]**	**L/H [-]**	**P/H [-]**	**S/H [-]**
		mean±standard deviation				
Poland	male	1.778±0.058	27.4±3.85	0.450±0.0115	0.194±0.0034	0.191±0.0024
	female	1.634±0.051	25.9±4.75	0.450±0.0115	0.219±0.0063	0.189±0.0057
United Kingdom	male	1.775±0.057	27.2±4.45	0.450±0.0115	0.205±0.0068	0.193±0.0025
	female	1.620±0.053	26.9±5.53	0.450±0.0115	0.241±0.0126	0.189±0.0013
USA	male	1.755±0.056	28.6±4.63	0.450±0.0115	0.196±0.0050	0.196±0.0015
	female	1.626±0.054	28.7±5.63	0.450±0.0115	0.217±0.0065	0.186±0.0020

(iii) Determination of the BMI based on the gamma distribution, and subsequently determination of the pedestrian mass, m.

(iv) Determination of the leg length, L, assuming the ratio $\frac{L}{H}$ is characterised by the normal distribution.

(v) Determination of the ratios $\frac{P}{H}$ and $\frac{S}{H}$ assuming normal distributions and relationships of these ratios with the BMI. The latter assumption was adopted to avoid outliers, e.g. pedestrians with wide pelvis but low mass or narrow shoulders but high mass. This was achieved by applying linear relationships expressed in Eq. 27, where μ and σ denote the mean and standard deviation, respectively.

$$\begin{aligned}
\mu_{P/H,mod} =& \mu_{P/H} + \frac{\sigma_{P/H}}{\sigma_{BMI}} (BMI - \mu_{BMI}) \\
\mu_{S/H,mod} =& \mu_{S/H} + \frac{\sigma_{S/H}}{\sigma_{BMI}} (BMI - \mu_{BMI}) \\
\sigma_{P/H,mod} =& \frac{\sigma_{P/H}}{2} \\
\sigma_{S/H,mod} =& \frac{\sigma_{S/H}}{2}
\end{aligned} \tag{27}$$

Due to availability, verification of the proposed statistical model was conducted based on the data from the English population reported by the NHS [62]. It can be seen in Figure 3 (a) that the BMI for men is only slightly skewed to the right, but the right tail is much longer for women, as seen in Figure 3 (b). This shape of the data distribution is captured by the gamma distribution, as assumed in (iii). A comparison of the output of the proposed statistical model in terms of body height, H, and mass, m, is shown in Figure 4. It can be seen that the body height and mass are captured by the statistical model very well for both men and women, but there is slightly higher variability of the body height obtained from the model relative to measurements. However, since the calibrated and generalised IPM gives more detrimental self-excited forces for shorter and heavier pedestrians, and the statistical model is slightly biased in these directions, it can be considered acceptable. This can be further understood by inspecting Figure 5, presenting the relationship between the coefficient of proportionality in the foot placement control law, α, and the body mass, m, based on the statistical model for the Polish population. The body mass, m, scales the magnitude of the equivalent added damping directly, as can be seen in Eq. 8. The lower the value of α, assuming all other relevant pedestrian anthropometric and gait characteristics, and structural lateral oscillatory motion remain the same, the stronger the influence of the lateral structural motion on the step width, as can be seen in Eq. 2.

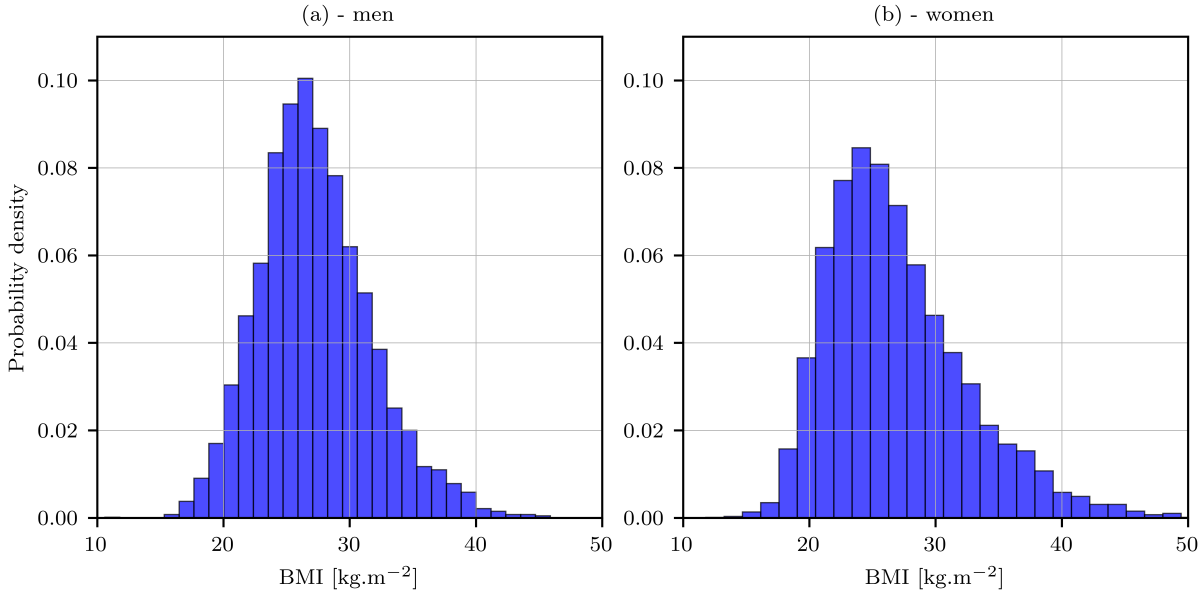

Figure 3: Distribution of the BMI of the English population according to the NHS data [62] and the statistical model.

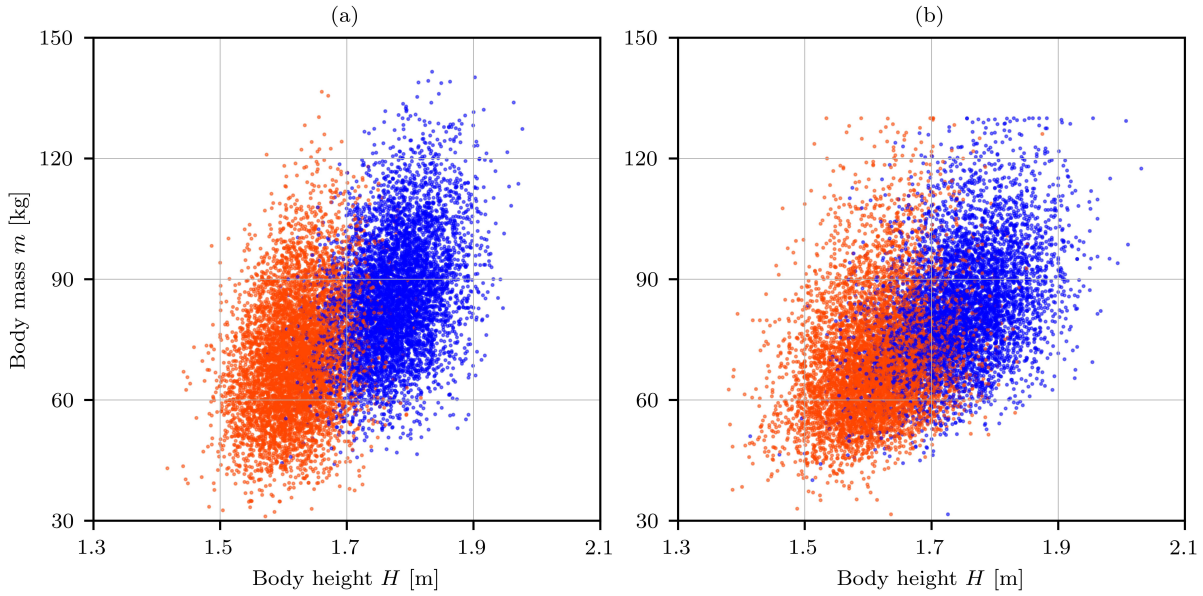

Figure 4: Comparison of the data from the English population obtained from the NHS [62] with the outputs from the statistical model in terms of the height, H, and body mass, m. The red and blue dots represent women and men, respectively.

3.3 Generalised IPM validity study

Having established the procedure for obtaining a statistical model of the anthropometric parameters of the considered population in Section 3.2, it is now possible to verify the applicability of the calibrated and generalised IPM for the range of its defining parameters. The underlying rationale for this task is that the predictions of the IPM are valid if the kinematic constraints associated with real walking gait are preserved.

The original IPM proposed by Macdonald [1] was derived based on the assumption of a small angle of the pendulum leg from vertical at the step switchover. That angle, θ, is denoted in Figure 6, together with the lateral distance between the locations of the CoP at consecutive steps, Δu. For some combinations of

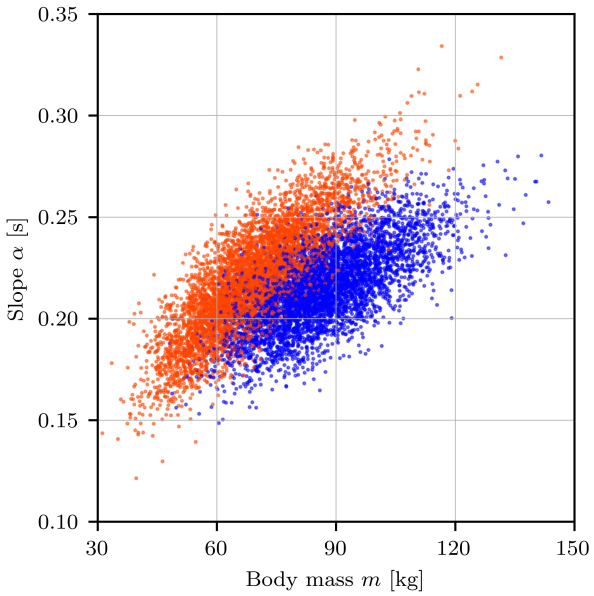

Figure 5: The relationship between the coefficient of proportionality in the foot placement control law, α, and the body mass, m, according to the statistical model for the Polish population. The red and blue dots represent women and men, respectively.

defining parameters, the IPM can generate the lateral CoM velocities translating into Δu which are not seen in real human gait, which violates the small angle assumption and invalidates the forces generated from the IPM. This issue is treated rigorously in this section.

The step width is increased for higher structural oscillation amplitudes, X, lower coefficient of proportionality, α, and higher free coefficient, β. The influence of the stride and structural oscillation frequencies, f_s and f_b, respectively, is more complex. However, lower f_s typically translates into an increased step width. Due to a relatively little influence on the setp width and to simplify the matter, β was taken as zero. The parameters α and f_b are predetermined by the pedestrian anthropometric parameters and structural characteristics (predominantly mass and stiffness), respectively. The structural oscillation amplitude, X, is an independent variable which does not affect the magnitudes of self-excited forces in Eqs. 8 and 9, however, it affects the step width. Since X during the instability period of the CMB [9] and CSB [10] reached approximately 0.01 m, this value was adopted in the subsequent analysis of the IPM applicability.

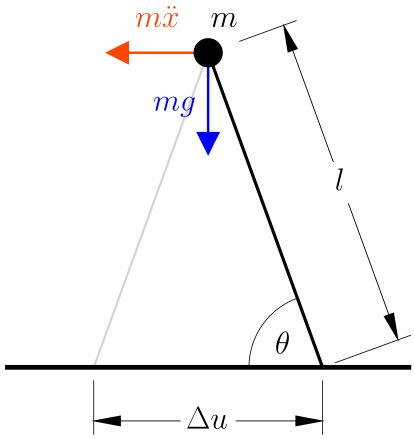

Figure 6: The IPM at the step transition – the lateral distance between the location of the centre of pressure (CoP) for consecutive steps, Δu, and the resulting angle of the stepping leg from vertical, θ.

A small angle approximation, enabling trigonometric functions to be avoided within the IPM solution, typically applies for angles up to 15 degrees. Although the accuracy of small angle approximation keeps decreasing beyond that value, a limit of 20 degrees was adopted herein reflecting the step widths which are still easily achievable in real human gait while not overly compromising the accuracy of the IPM relative to the exact solution. This can be understood by inspecting the Taylor series approximation for $\sin\theta$, which contains only odd components, i.e. $\theta - \frac{\theta^3}{3!} + \frac{\theta^5}{5!} - (...)$. According to this assumption, $\theta \geq \frac{7}{18}\pi$ which means that $\frac{\Delta u}{2l} \leq \cos\frac{7}{18}\pi \approx 0.342$. Therefore, assuming $l = 1.34L$ as taken in Macdonald [1], where l is the pendulum length, the condition that must be satisfied is as follows:

$$|\Delta u| \leq 0.9166L \tag{28}$$

Adopting the assumption $\beta = 0$, the change in the lateral position of the CoP between consecutive steps can be calculated according to Eq. 31 in Czaplewski & Bocian [3]:

$$\Delta u = \left[A\left(\alpha\dot{x}_0 + x_0\right) - \alpha\tilde{\dot{x}}_0\right] e^{(2\alpha f_s)^{-1}} - A\left(\alpha\dot{x}_1 + x_1\right) + \alpha\tilde{\dot{x}}_1 \tag{29}$$

where $A = 1 - \frac{1}{1+\alpha^2\omega_b^2}$ and:

$$\begin{aligned}
x_0 &= X\sin\left(\psi - \psi_p\right)\\
\dot{x}_0 &= X\omega_b\cos\left(\psi - \psi_p\right)\\
\tilde{\dot{x}}_0 &= X\omega_b\cos\left(\psi - \psi_p - \psi_\tau\right)\\
x_1 &= X\sin\psi\\
\dot{x}_1 &= X\omega_b\cos\psi\\
\tilde{\dot{x}}_1 &= X\omega_b\cos\left(\psi - \psi_\tau\right)
\end{aligned} \tag{30}$$

where ψ is the bridge phase angle, and $\psi_p = \frac{\omega_b}{2f_s}$ and $\psi_\tau = \omega_b\tau$ are phase offsets as per period of a single step and per time offset τ, respectively. Δu is at maximum when:

$$\psi = 2\left[\arctan\left(\frac{\sqrt{C_1^2 + C_2^2} + C_2}{C_1}\right) + \pi\right] = \psi^* \tag{31}$$

where:

$$\begin{aligned}
C_1 = {} & \left(-A\alpha\omega_b\cos\psi_p + A\sin\psi_p - \alpha\omega_b\sin\psi_p\sin\psi_\tau + \alpha\omega\cos\psi_p\cos\psi_\tau\right) e^{(2\alpha fs)^{-1}} + A\alpha\omega_b + \alpha\omega_b\cos\psi_\tau\\
C_2 = {} & \left(A\alpha\omega_b\sin\psi_p + A\cos\psi_p - \alpha\omega_b\sin\psi_p\cos\psi_\tau - \alpha\omega_b\cos\psi_p\sin\psi_\tau\right) e^{(2\alpha fs)^{-1}} - A - \alpha\omega_b\sin\psi_\tau
\end{aligned} \tag{32}$$

The maximum separation between the lateral position of the CoP, Δu^*, is then:

$$\begin{aligned}
\Delta u^* = X\Big|\Big\{A\big[\alpha\omega_b(\sin\psi_p\sin\psi^* + \cos\psi_p\cos\psi^*) + \cos\psi_p\sin\psi^* - \sin\psi_p\cos\psi^*\big] +\\
- \alpha\omega_b\big[(\cos\psi_p\sin\psi_\tau + \sin\psi_p\cos\psi_\tau)\sin\psi^* + (\cos\psi_p\cos\psi_\tau - \sin\psi_p\sin\psi_\tau)\cos\psi^*\big]\Big\}e^{(2\alpha f_s)^{-1}} +\\
- A(\alpha\omega_b\cos\psi^* + \sin\psi^*) + \alpha\omega_b(\sin\psi_\tau\sin\psi^* + \cos\psi_\tau\cos\psi^*)\Big|
\end{aligned} \tag{33}$$

Δu^* defined in Eq. 28 is a characteristic value for any combination of α and ω_b. It is now necessary to reverse the problem and find the minimum f_s for which Eq. 28 is satisfied. The exemplar results from the analysis of the IPM validity are presented in Figure 7. The leg length, L, was established from α while adopting the average L/H, P/H and S/H based on the representative sample of the Polish population. The presented results can be evaluated in the context of typical pedestrian stride frequencies which fall between 0.6 and 1.1 Hz. It can be seen that the applicability of the IPM is generally limited at the combination of the lowest α and f_b within the range of 0.3 to 1.3 Hz and, more significantly, at f_b close to 2 Hz. The importance of these parametric limits can be understood by considering the range of α for the representative sample of the Polish population presented in Figure 5 and the stepping behaviour of pedestrians walking on a laterally-oscillating instrumented treadmill reported in [18], [19].

Small values of α, below 0.17 s, can be seen in Figure 5 for the pedestrians having the lowest mass, who comprise a small part of the whole population. Furthermore, when subjected to the lateral structural motion, pedestrians have a tendency to speed up their steps, i.e. increase their stepping rate. The results from the tests reported in [18], [19] show that the lowest average stride frequency was above 0.8 Hz. Importantly, those results come from an experimental setup enabling pedestrians to freely adjust their walking speed, hence stride frequency, due to the incorporated automatic treadmill belt speed feedback mechanism. This justifies the cases for which the combination of parameters defining the IPM violates the lateral CoP separation condition to be treated as outliers and omitting them from further analyses.

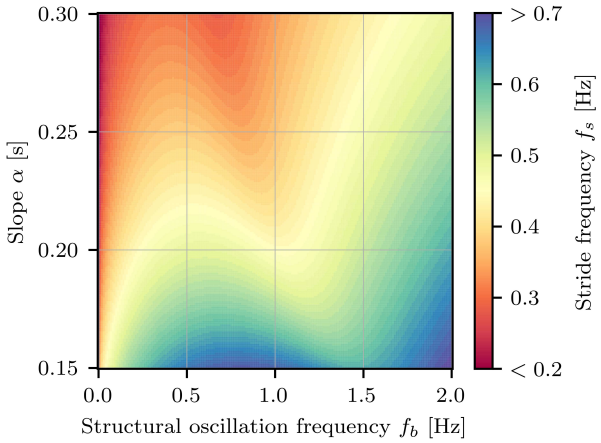

Figure 7: The minimum stride frequency, f_s, for which the IPM provides valid solutions based on the representative sample of the Polish population.

3.4 Critical structural dynamic stability parameters

The critical structural dynamic stability parameters were established following the methodology introduced in Bocian et al. [5]. The normalised mean equivalent added damping, $\tilde{\mu}_{\Delta C}$, normalised standard deviation of the equivalent added damping, $\tilde{\sigma}_{\Delta C}$, and mean normalised equivalent added mass, $\tilde{\mu}_{\Delta M}$, were obtained using Eqs. 8, 9 and 19, respectively. The range of structural oscillation frequency, f_b, was taken as [0.001 Hz, 2.0 Hz]. The upper limit of f_b was chosen conservatively since no cases of pedestrian-induced lateral dynamic instability have been reported beyond $f_b \approx 1.12$ Hz (see Table 1 in [38]), except from a single case of the Cragside Bridge opened in 1875, which is a wrought iron arch bridge having extremely low lateral stiffness and the main lateral mode at approximately 2.8 Hz [64]. Furthermore, the UK National Annex to Eurocode 1 [35], which arguably contains the most sophisticated provisions for designing structures against pedestrian-induced lateral instability currently available, states that it may be assumed that unstable lateral response will not occur for structures not having significant lateral modes below 1.5 Hz. The range of pedestrian walking speed, v, was taken as [0.6 ms^{-1}, 1.7 ms^{-1}]. The lower limit of v represents the pedestrian walking speed in a crowd at density of approximately 2 people/m^2 [6], [52] beyond which walking is heavily impaired.

The upper limit represents the speed at which a pedestrian is highly likely to change their gait from walking to running. The stride frequency, f_s, for each pedestrian from a representative sample of the considered population of the size $N = 10000$ was obtained from the relationship established in Dean (1965) [65]:

$$f_s = 1.3502 \frac{v^{0.5}}{H} \tag{34}$$

The stride frequency was verified and corrected, if necessary, according to the procedure outlined in Section 3.3. The values of $-\tilde{\mu}_{\Delta C}$, $\tilde{\sigma}_{\Delta C}$ and $\tilde{\mu}_{\Delta M}$, together with their corresponding extreme values for each considered f_b are shown in Figure 8. It needs to be pointed out that $\tilde{\mu}_{\Delta C}$, defined in Eq. 14, is presented in Figure 8 with a reversed sign, since this is how it enters the probabilistic stability criteria presented in Section 2.3.

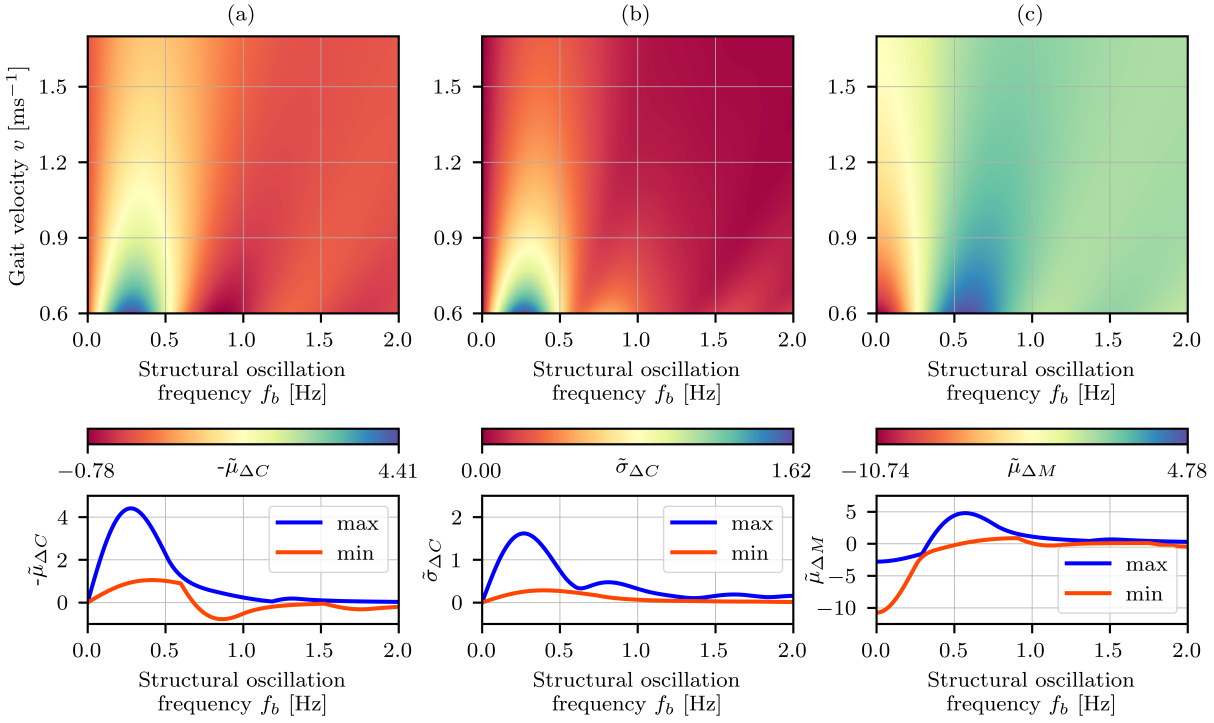

Figure 8: (a) The normalised mean equivalent added damping, (b) the corresponding standard deviation of the equivalent added damping, and (c) the normalised mean equivalent added mass. The plots in the top row present the results relative to the walking speed and the plots in the bottom row present the envelopes of the minimum and maximum values.

In general, the extreme values of parameters shown in Figure 8 were obtained for the lowest walking speeds. The extreme values of $-\tilde{\mu}_{\Delta C}$ are always positive for f_s smaller than approximately 0.7 Hz, and $-\tilde{\mu}_{\Delta C}$ can take values above 4 for f_b between approximately 0.2 Hz and 0.3 Hz. For f_b above 0.7 Hz, the maximum and minimum values of $-\tilde{\mu}_{\Delta C}$ are always positive and negative, respectively, having magnitude below 1, except for f_b at around 1.2 Hz for which the maximum is 0.

The maximum $\tilde{\sigma}_{\Delta C}$ at approximately 1.6 is found for f_b corresponding to the maximum of $-\tilde{\mu}_{\Delta C}$. For f_b above 0.6 Hz $\tilde{\sigma}_{\Delta C}$ is generally below 0.5.

For f_b below 0.3 Hz $\tilde{\mu}_{\Delta M}$ is always negative, but for f_b between approximately 0.5 Hz and 1 Hz it is always positive. The global minimum of $\tilde{\mu}_{\Delta M}$ at approximately -10 is found for the lowest considered f_b close to 0 Hz, and the global maximum of $\tilde{\mu}_{\Delta M}$ at approximately 5 is found for f_b at approximately 0.6 Hz. For f_b beyond approximately 0.8 Hz $\tilde{\mu}_{\Delta M}$ takes values between -0.5 and 2.

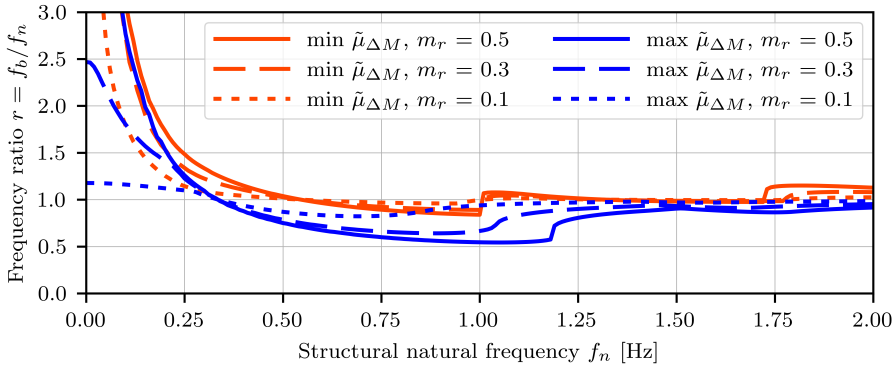

Figure 9: Frequency ratio, $r = \frac{f_b}{f_n}$.

3.4.1 Frequency shifts due to the equivalent added mass effect

The effect of the equivalent added mass is to shift the vibration frequency of the structure subjected to the loading from pedestrians. Having obtained the envelopes of minimum and maximum values of $\tilde{\mu}_{\Delta M}$ presented in Figure 8, it was possible to determine the corresponding frequency shifts, $r = \frac{f_b}{f_n}$, according to Eq. 11. For clarity of the presentation, the pedestrian-to-structure mass ratio, m_r, was taken as 0.1, 0.3 and 0.5. Since the maximum mass ratio observed on bridges during the lateral dynamic structural instability period was approximately 0.23 for the LMF [6] (assuming uniform distribution of pedestrians on the bridge), the value of $m_r = 0.3$ conservatively covers all known cases. The results of this analysis are shown in Figure 9. It needs to be borne in mind that the presented frequency shifts may not correspond to the critical conditions for structural instability. However, they are indicative of the possible changes in the structural vibration frequency due to the presence of pedestrians. For f_n below 0.3 Hz, r is always higher than 1 or it is undefined. In all these cases the presence of pedestrians increases the structural vibration frequency, f_b, relative to the natural frequency, f_n, meaning that pedestrians act in this case as a source of significant negative mass to the structure. For f_n between approximately 0.5 Hz and 1.5 Hz, r is usually smaller than 1, dropping to as little as 0.5, which means that the pedestrians act in this case as a source of significant additional mass to the structure.

3.4.2 Critical added damping

Having established the frequency shifts for the considered range of pedestrian walking speeds, v, and pedestrian-to-bridge mass ratios, m_r, it is now possible to define $-\tilde{\mu}_{\Delta C}$ accounting for the frequency shifts and expressed relative to the natural structural frequency, f_n. Due to the frequency shifts associated with the equivalent added mass effect discussed in Section 3.4.1, the critical $-\tilde{\mu}_{\Delta C}$ was sometimes found at multiple values for a single f_n. In these cases the maximum (positive) value of $-\tilde{\mu}_{\Delta C}$ was preserved, since it is the most detrimental to structural stability. The results for $-\tilde{\mu}_{\Delta C}$ are shown in Figure 10 (a), and the corresponding $\tilde{\sigma}_{\Delta C}$ is shown in Figure 10 (b). The most interesting results are obtained for f_n up to 1.2 Hz, i.e. for the range of f_n containing modal frequencies for which instability was identified from full-scale bridges. In this case, the higher m_r, the wider the range of f_n for which $-\tilde{\mu}_{\Delta C}$ is positive. Beyond $f_n \approx 1$ Hz, there is relatively little variation of $-\tilde{\mu}_{\Delta C}$, of which magnitude is generally low. As could be expected (see the discussion of Figure 8 in Section 3.4), the critical $-\tilde{\mu}_{\Delta C}$ is found, in most cases, for the lowest v. The exception is the interval of f_n defined by the intersection points of curves representing the lowest and the highest walking speeds. Therefore, results for the lowest and highest v (0.6 ms^{-1} and 1.7 ms^{-1}, respectively) only need to be considered to derive simplified envelopes of $-\tilde{\mu}_{\Delta C}$ and $\tilde{\sigma}_{\Delta C}$ for use with the probabilistic stability criteria presented in Section 2.3.

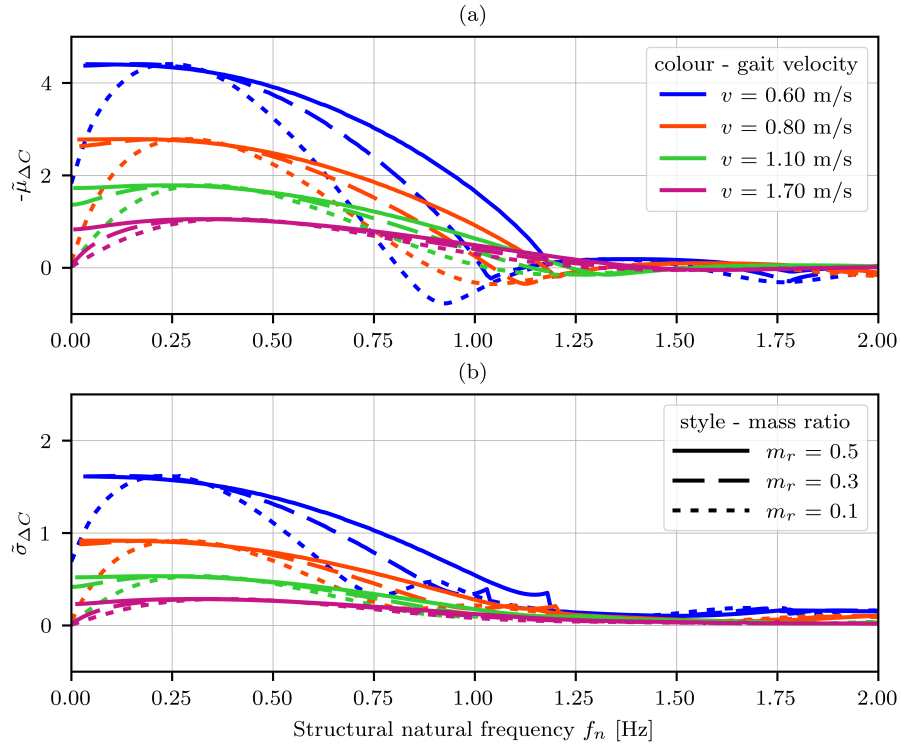

Figure 10: The relationship between the structural natural frequency, f_n, and (a) $-\tilde{\mu}_{\Delta C}$ and (b) $\tilde{\sigma}_{\Delta C}$ accounting for the considered range of walking speeds, v, and mass ratios, m_r. The legends apply to both plots.

3.4.3 Piecewise-linear envelopes for the critical added damping

The results presented in Figure 10 are defined by curves which cannot be expressed using simple functions. However, simplicity is a desired characteristic of any structural design guidelines since it generally makes them easier to apply hence prevents from making errors. Therefore, simplified envelopes were established for the relationships between $-\tilde{\mu}_{\Delta C}$ and f_n, and $\tilde{\sigma}_{\Delta C}$ and f_n. A systematic approach was adopted in this process, according to the procedure introduced hereafter, to avoid arbitrariness and ensuring universal applicability, e.g. for various populations of pedestrians. The development of piecewise-linear envelopes for $-\tilde{\mu}_{\Delta C}$ and $\tilde{\sigma}_{\Delta C}$ based on $m_r = 0.3$, which encompasses all known mass ratios for the recorded cases of lateral structural instability, is presented in Figure 11.

The piecewise-linear envelope of $-\tilde{\mu}_{\Delta C}$ presented in Figure 11 (a) consists of five sections, three of which describe linearly varying values and the remaining two set at constant values. These constant values, denoted $-\tilde{\mu}_{\Delta C,const,1}$ and $-\tilde{\mu}_{\Delta C,const,2}$, were determined by finding the first two local maxima of $-\tilde{\mu}_{\Delta C}$ expressed relative to f_b, as shown in Figure 12 (a). Deriving these values from the relationship of $-\tilde{\mu}_{\Delta C}$ with f_b rather than f_n was convenient and acceptable, since the local maxima within the considered range of f_b and f_n are independent of m_r.

The first section describing linearly varying values was obtained by finding a tangential line to $-\tilde{\mu}_{\Delta C}$ for $v = 0.6\ \mathrm{m\,s^{-1}}$ at the first f_n for which $-\tilde{\mu}_{\Delta C} = 0$, as denoted in Figure 11 (a) by the green dot. That tangential line is denoted in Figure 11 (a) in green and it is given by:

$$\tilde{\mu}_{\Delta C,lin,1}(f_n) = a_{\mu,1}(m_r) f_n + b_{\mu,1}(m_r) \tag{35}$$

where the parameters $a_{\mu,1}$ and $b_{\mu,1}$ are dependent on m_r.

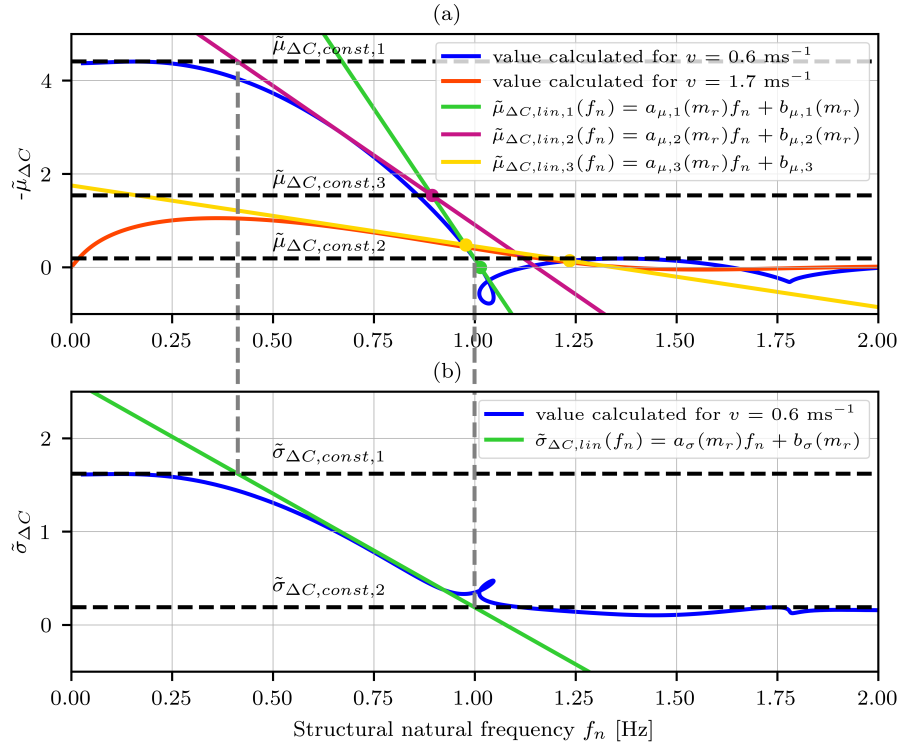

Figure 11: Development of the piecewise-linear envelopes for the critical $-\tilde{\mu}_{\Delta C}$ and $\tilde{\sigma}_{\Delta C}$ at $m_r = 0.3$.

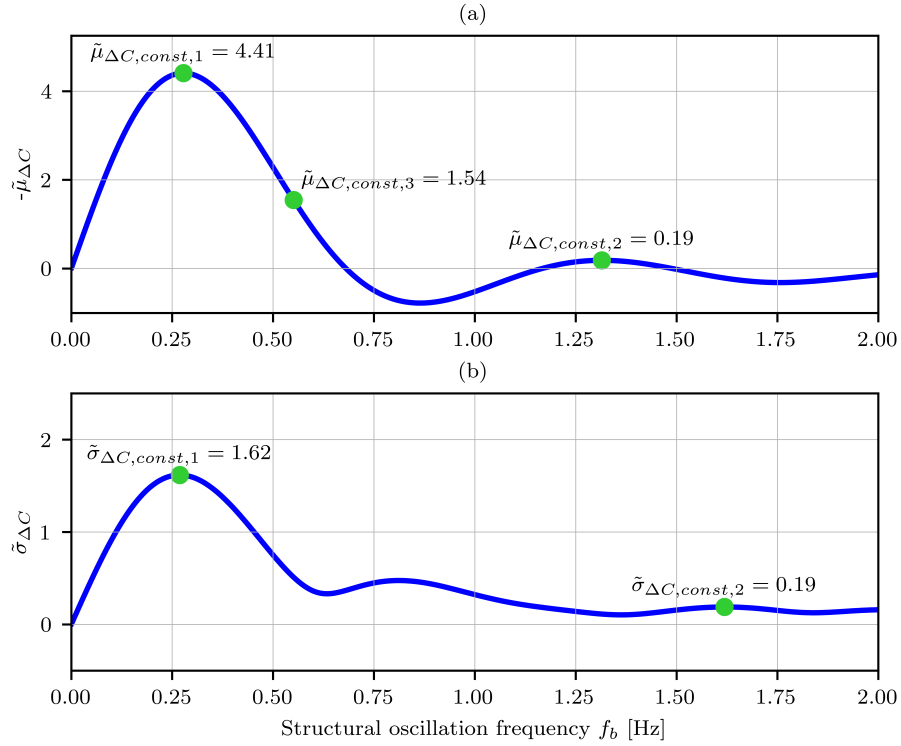

Figure 12: Characteristic values of $-\tilde{\mu}_{\Delta C}$ and $\tilde{\sigma}_{\Delta C}$ used in the derivation of the piecewise linear envelopes of $-\tilde{\mu}_{\Delta C}$ and $\tilde{\sigma}_{\Delta C}$ presented in Figure 11.

The second section describing linearly varying values was obtained by finding a tangential line to $-\tilde{\mu}_{\Delta C}$ for $v = 0.6$ m s^{-1} passing through the point denoted in Figure 11 (a) by the purple dot. That point is at the intersection of the green tangential line previously obtained and $-\tilde{\mu}_{\Delta C,const,3}$ obtained from Figure 11 (a).

The ordinate of that point was taken as a fraction k_μ of $\max(-\tilde{\mu}_{\Delta C})$, where k_μ was adopted as 0.35. The second section describing linearly varying values is denoted in Figure 11 (a) in purple and it is given by:

$$\tilde{\mu}_{\Delta C,lin,2}(f_n) = a_{\mu,2}(m_r)f_n + b_{\mu,2}(m_r) \tag{36}$$

where the parameters $a_{\mu,2}$ and $b_{\mu,2}$ are dependent on m_r.

The third section describing linearly varying values was obtained by connecting the first two intersection points of the curves for $-\tilde{\mu}_{\Delta C}$ for $v = 0.6\ \mathrm{m\,s^{-1}}$ and $-\tilde{\mu}_{\Delta C}$ for $v = 1.7\ \mathrm{m\,s^{-1}}$. This section is delimited within Figure 11 by the two yellow dots and it is given by:

$$\tilde{\mu}_{\Delta C,lin,3}(f_n) = a_{\mu,3}(m_r)f_n + b_{\mu,3} \tag{37}$$

The crossing points of the first line describing linearly varying values with the line set at a constant value of $-\tilde{\mu}_{\Delta C}$ representing the second local maximum, and the second line describing linearly varying values with the line set at a constant value of $-\tilde{\mu}_{\Delta C}$ representing its maximum, all presented in Figure 11 (a), denote the limiting values of f_n used in defining the envelope of $\tilde{\sigma}_{\Delta C}$ presented in Figure 11 (b). To make it clear, dashed vertical lines were denoted therein, linking the specified values. For f_n on the left and right side of the crossing points described above, the envelope of $\tilde{\sigma}_{\Delta C}$ takes constant values equal to the first and third local maximum of $\tilde{\sigma}_{\Delta C}$, respectively, which are denoted in Figure 12 (b) by green dots. The second local maximum in Figure 12 (b) is discarded since it corresponds to the range in which $-\tilde{\mu}_{\Delta C}$ is negative (see Figures 11 and 12). The section describing linearly varying values of $\tilde{\sigma}_{\Delta C}$, denoted in Figure 11 (b) in green, is constructed by linking the sections for which the envelope of $\tilde{\sigma}_{\Delta C}$ is constant, and it is given by:

$$\tilde{\sigma}_{\Delta C,lin}(f_n) = a_\sigma(m_r)f_n + b_\sigma(m_r) \tag{38}$$

where the parameters a_σ and b_σ depend on m_r.

The parameters $a_{\mu,1}$, $b_{\mu,1}$, $a_{\mu,2}$, $b_{\mu,2}$, $a_{\mu,3}$, a_σ, b_σ, used in Eqs. 35, 36, 37 and 38, were obtained for each m_r within the range [0.10, 0.11, (...) , 0.50], by approximation with 3rd order polynomials. The parameter $b_{\mu,3}$ was taken as constant and invariant of m_r.

For the given f_n and m_r, the envelopes of the critical mean equivalent added damping, $\tilde{\mu}_{\Delta C}$, and the critical standard deviation of the mean equivalent added damping, $\tilde{\sigma}_{\Delta C}$, are obtained from equations presented in Table 3. Exemplar envelopes based on data for the Polish population are presented in Figure 13 for mass ratios $m_r = 0.1$ in (a) & (d), $m_r = 0.3$ in (b) & (e) and $m_r = 0.5$ in (c) & (f). It can be seen that the higher the mass ratio, m_r, the wider the range of frequencies, f_n, for which significant negative damping effect can occur.

3.5 Validation study

This section presents exemplar applications of the proposed lateral dynamic stability criteria based on the case studies of the Clifton Suspension Bridge (CSB) in the UK [10], [12] and the Squibb Park Bridge (SPB) in the USA [66]. These two bridges – CSB and SPB – differ with respect to their primary function – as they carry mixed and pedestrian traffic only, scale – having the main span of 194 m and 37 m, structural arrangement – supported by classical chain suspension system and underslung system, and the construction era – industrial revolution and recent decades. However, they were both found susceptible to pedestrian-induced lateral dynamic instability, although for different loading intensities – hundreds of pedestrians and

Table 3: The piecewise-linear envelopes of the critical mean equivalent added damping, $\tilde{\mu}_{\Delta C}$, and standard deviation, $\tilde{\sigma}_{\Delta C}$, for the populations of Poland, the UK and the USA.

Poland	**United Kingdom**	**USA**
$\tilde{\mu}_{\Delta C,calc}(f_n, m_r) = \max\{\tilde{\mu}_{\Delta C,const,2}, \min\{\tilde{\mu}_{\Delta C,lin,1}(f_n, m_r), \tilde{\mu}_{\Delta C,lin,2}(f_n, m_r), \tilde{\mu}_{\Delta C,const,1}\}, \tilde{\mu}_{\Delta C,lin,3}(f_n, m_r)\}$ $\tilde{\sigma}_{\Delta C,calc}(f_n, m_r) = \max\{\tilde{\sigma}_{\Delta C,const,2}, \min\{\tilde{\sigma}_{\Delta C,lin}(f_n, m_r), \tilde{\sigma}_{\Delta C,const,1}\}\}$		
$\tilde{\mu}_{\Delta C,const,1} = 4.41$ $\tilde{\mu}_{\Delta C,const,2} = 0.19$ $\tilde{\sigma}_{\Delta C,const,1} = 1.62$ $\tilde{\sigma}_{\Delta C,const,2} = 0.19$	$\tilde{\mu}_{\Delta C,const,1} = 3.17$ $\tilde{\mu}_{\Delta C,const,2} = 0.14$ $\tilde{\sigma}_{\Delta C,const,1} = 1.18$ $\tilde{\sigma}_{\Delta C,const,2} = 0.13$	$\tilde{\mu}_{\Delta C,const,1} = 4.16$ $\tilde{\mu}_{\Delta C,const,2} = 0.17$ $\tilde{\sigma}_{\Delta C,const,1} = 0.98$ $\tilde{\sigma}_{\Delta C,const,2} = 0.29$
$\tilde{\mu}_{\Delta C,lin,1}(f_n, m_r) = a_{\mu,1}(m_r) f_n + b_{\mu,1}(m_r)$ $\tilde{\mu}_{\Delta C,lin,2}(f_n, m_r) = a_{\mu,2}(m_r) f_n + b_{\mu,2}(m_r)$ $\tilde{\mu}_{\Delta C,lin,3}(f_n, m_r) = a_{\mu,3}(m_r) f_n + b_{\mu,3}$ $\tilde{\sigma}_{\Delta C,lin}(f_n, m_r) = a_{\sigma}(m_r) f_n + b_{\sigma}(m_r)$		
$a_{\mu,1}(m_r) = 16.97 m_r^3 - 4.14 m_r^2 - 10.02 m_r - 9.94$ $b_{\mu,1}(m_r) = -20.19 m_r^3 + 8.29 m_r^2 + 20.3 m_r + 6.75$ $a_{\mu,2}(m_r) = 135.39 m_r^3 - 165.72 m_r^2 + 73.43 m_r - 16.67$ $b_{\mu,2}(m_r) = -63.48 m_r^3 + 76.32 m_r^2 - 32.23 m_r + 11.35$ $a_{\mu,3}(m_r) = 0.17 m_r^3 - 0.43 m_r^2 + 0.63 m_r - 1.45$ $b_{\mu,3} = 1.74$ $a_{\sigma}(m_r) = 27.61 m_r^3 - 34.94 m_r^2 + 16.82 m_r - 5.07$ $b_{\sigma}(m_r) = -14.53 m_r^3 + 17.78 m_r^2 - 7.8 m_r + 3.75$	$a_{\mu,1}(m_r) = 82.05 m_r^3 - 85.9 m_r^2 + 22.25 m_r - 9.27$ $b_{\mu,1}(m_r) = -40.95 m_r^3 + 46.45 m_r^2 - 5.47 m_r + 6.14$ $a_{\mu,2}(m_r) = -61.23 m_r^3 + 37.67 m_r^2 + 6.46 m_r - 9.0$ $b_{\mu,2}(m_r) = 49.65 m_r^3 - 39.32 m_r^2 + 4.73 m_r + 6.08$ $a_{\mu,3}(m_r) = 0.47 m_r^3 - 0.6 m_r^2 + 0.5 m_r - 1.13$ $b_{\mu,3} = 1.33$ $a_{\sigma}(m_r) = -16.63 m_r^3 + 11.14 m_r^2 + 1.1 m_r - 2.95$ $b_{\sigma}(m_r) = 18.49 m_r^3 - 16.27 m_r^2 + 3.19 m_r + 2.03$	$a_{\mu,1}(m_r) = 57.2 m_r^3 - 43.97 m_r^2 + 2.3 m_r - 9.94$ $b_{\mu,1}(m_r) = -20.3 m_r^3 + 14.71 m_r^2 + 14.53 m_r + 6.6$ $a_{\mu,2}(m_r) = 120.91 m_r^3 - 149.34 m_r^2 + 67.3 m_r - 15.69$ $b_{\mu,2}(m_r) = -49.57 m_r^3 + 63.14 m_r^2 - 28.42 m_r + 10.68$ $a_{\mu,3}(m_r) = -0.23 m_r^3 + 0.03 m_r^2 + 0.44 m_r - 1.35$ $b_{\mu,3} = 1.67$ $a_{\sigma}(m_r) = 11.99 m_r^3 - 15.3 m_r^2 + 7.55 m_r - 2.4$ $b_{\sigma}(m_r) = -5.31 m_r^3 + 7.01 m_r^2 - 3.35 m_r + 1.99$

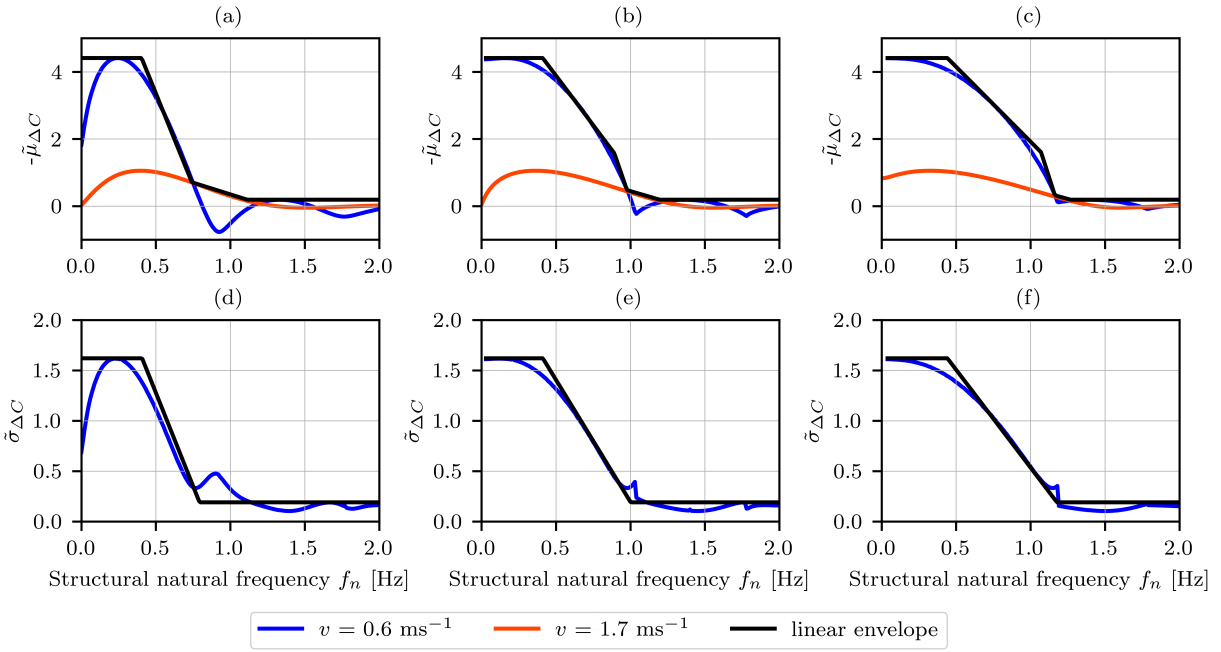

Figure 13: Exemplar piecewise linear envelopes of $-\tilde{\mu}_{\Delta C}$ and $\tilde{\sigma}_{\Delta C}$, respectively, for $m_r = 0.1$ in (a) & (b), $m_r = 0.3$ in (c) & (d), and $m_r = 0.5$ in (e) & (f), based on a representative sample of the Polish population, as defined in Table 3.

few pedestrians only for the CSB and SPB, respectively. The SPB is introduced herein in more detail, since it is relatively little known in the structural engineering community. The results from direct (CSB) and indirect (SPB) measurements of the dynamic behaviour of these bridges and simulations described herein served to evaluate the proposed structural lateral dynamic stability criteria. For each bridge, numerous simulations were run to determine lateral structural response due to walking pedestrians in the same way as in [52] and [2], considering each mode independently and pedestrian force accounting for all components, i.e. self-excited forces and F_{rem} as defined in Eq. 1. According to the calibrated and generalised IPM [2], the behaviour of each pedestrian is given by:

$$\ddot{y}_i + \frac{u_{i,j} - y_i}{\alpha_i^2} = -\phi_i \ddot{X} \tag{39}$$

where X is the generalised displacement of analysed mode, and ϕ is the mode shape amplitude denoted here such that ϕ_i is the mode shape amplitude at the location of i-th pedestrian. The behaviour of the bridge is given by:

$$\ddot{X} + 2\omega_n \zeta \dot{X} + \omega_n^2 X = \frac{1}{M} \sum_{i=1}^{N} \frac{\phi_i m_i}{\alpha_i^2} (u_{i,j} - y_i) \tag{40}$$

where ζ is the damping ratio, M is the modal mass and N is the number of pedestrians on the bridge. The distributions of pedestrians' anthropometric parameters were obtained from the statistical models of relevant populations according to the procedures presented in Section 3.2. The distribution of pedestrian walking speed, v, was taken according to the normal distribution, $\mathcal{N}(v, 0.05v)$ ms^{-1}. All simulations were run in Python 3.11. The results were compared with the formulas defining the lateral dynamic stability criteria presented in Section 2.3 based on $-\tilde{\mu}_{\Delta C}$ and $\tilde{\sigma}_{\Delta C}$ derived from the relevant populations, such as those presented in Figure 10, and also based on the piecewise linear envelopes of $-\tilde{\mu}_{\Delta C}$ and $\tilde{\sigma}_{\Delta C}$ proposed

in Section 3.4.3, and measurements from the relevant bridges. Structural instability was identified in simulations when the lateral vibration amplitudes reached above 10 mm. This corresponds to the modal lateral oscillation amplitude of the CSB during the instability period reported in [10]. It needs to be noted that the self-excited forces derived from the calibrated and generalised IPM are independent of the structural oscillation amplitude, hence they can be expressed as equivalent added damping and mass.

Determination of the stability criteria was conducted according to the pedestrian Scruton number defined in Eq. 16, accounting for various pedestrians' distributions on the bridge as captured by Eqs. 20, 24 and 26. This is a multi-step process due to the dependency of these equations on the mass ratio, m_r, and the number of pedestrians on the bridge, N, but also due to back-calculation of the natural frequency of the bridge given the response frequency. Therefore, to streamline this process, the approach to obtaining stability criteria will be individually tailored to the considered case studies. To establish a relationship between D and N_{cr}, denoting the critical number of pedestrians, i.e. the minimum number of pedestrians for which instability will occur, the stability boundaries for each bridge are expressed it terms of D and N_{cr}.

3.5.1 Clifton Suspension Bridge

Clifton Suspension Bridge (CSB) inaugurated in 1864 in Bristol, UK, is a chain suspension bridge designed by one of the forefathers of modern bridge engineering - Isambard Kingdom Brunel. The behaviour of the CSB during crowd loading was investigated by Macdonald [10] and others [12]. The bridge repeatedly suffered from excessive lateral vibrations when occupied by pedestrians during the annual International Baloon Fiesta. The instability was identified during this event in 2003 for two lateral modes at frequencies of 0.524 Hz (second lateral mode) and 0.746 Hz (third lateral mode), having damping ratios of 0.58% and 0.68%, respectively [10]. The dynamic stability of these modes is investigated herein. The length of the bridge was taken as 194 m and the mode shapes were taken from Figure 2 and Table 1 in [12]. The modal mass was obtained from a finite element model as 691.9 t and 698.7 t for the second and third lateral mode, respectively [10]. The distributions of pedestrians' anthropometric parameters for use within the calibrated IPM were obtained from the statistical model of the British population presented in Section 3.2. To ensure validity of the generalised IPM, excessive separation between the lateral foot placement and the CoM position was prevented using the procedure introduced in the parametric study presented in Section 3.3. However, the lateral vibration amplitude was adopted herein directly from the simulations rather than fixed as in Eq. 33. Exactly 100 simulations were conducted for each mode, randomly sampling the walking speed from the closed interval from 0.6 ms^{-1} to 1.7 ms^{-1} and the number of pedestrians on the bridge from the closed intervals from 35 to 235 and 100 to 500 for the second and third lateral mode, respectively.

To obtain the analytical solutions based on $-\tilde{\mu}_{\Delta C}$ and $\tilde{\sigma}_{\Delta C}$ presented in Figure 10, m_r was first established for a given N to determine corresponding $-\tilde{\mu}_{\Delta C}$ already including the added mass effect. Such obtained $-\tilde{\mu}_{\Delta C}$ is analogous to the pedestrian Scruton number, D, for uniform pedestrians' distribution on the bridge at 50% confidence limit, i.e. taking $z_{\gamma=0.5} = 0$. In this case, Eq. 22 can be expressed in terms of the critical number of pedestrians, N_{cr}, by substituting Eq. 23:

$$N_{cr} = -\frac{2\zeta M}{\tilde{\mu}_{\Delta C}\mu_m} \tag{41}$$

The stability boundaries for the second and third lateral mode of the CSB, respectively, are presented in Figure 14 (a) and (b) in terms of pedestrian Scruton number, D, and in Figure 15 (a) and (b) in terms of the critical number of pedestrians, N_{cr}. Instability will occur for any D below the stability boundary in Figure 14 and for $N \geq N_{cr}$ in Figure 15.

It can be seen in Figure 14 that for both modes and all considered pedestrian distributions, the results based on piecewise-linear envelopes, denoted with the subscript *env* on the plots, are invariant with respect to the

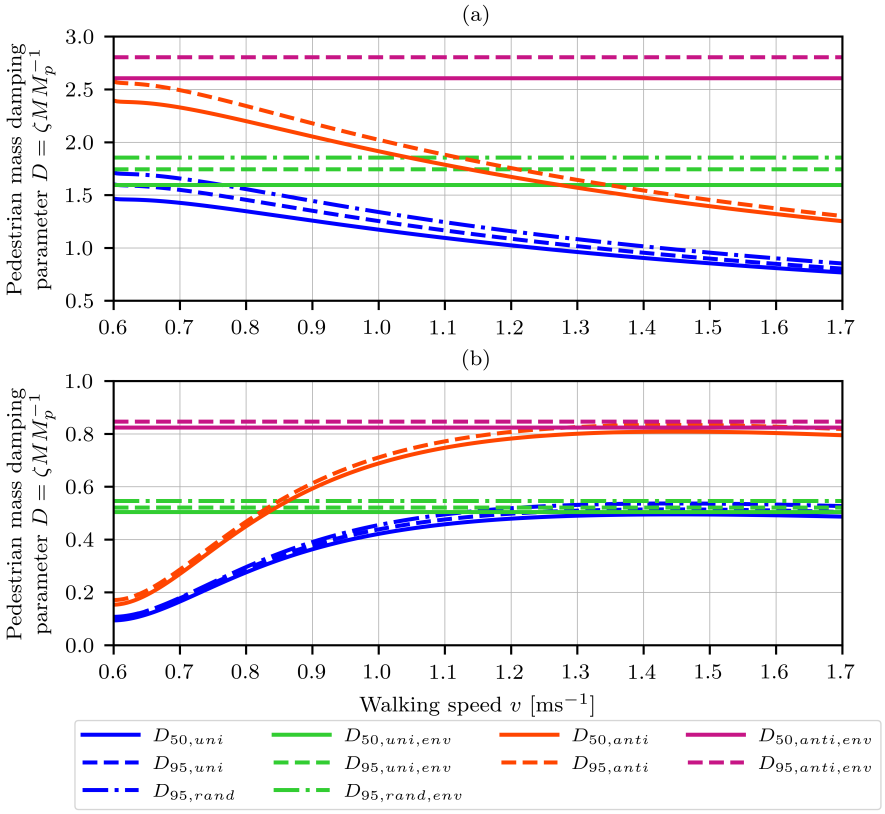

Figure 14: Pedestrian Scruton number, D, relative to the walking speed of pedestrians for the (a) second and (b) third lateral mode of the CSB based on the analytical solutions of $-\tilde{\mu}_{\Delta C}$ and $\tilde{\sigma}_{\Delta C}$, and their piecewise-linear envelopes.

walking speed, v. These results are almost always conservative relative to the corresponding results obtained from the exact solutions of $-\tilde{\mu}_{\Delta C}$ and $\tilde{\sigma}_{\Delta C}$. In the latter case, the highest and lowest D for the second lateral mode occurs for the lowest and highest v, respectively. However, the opposite relationship is found for the third lateral mode. As can be expected from the results for D obtained from the exact solutions for $-\tilde{\mu}_{\Delta C}$ and $\tilde{\sigma}_{\Delta C}$, N_{cr} is the lowest for the lowest and highest v for the second and third lateral mode, respectively, as shown in Figure 15. The most demanding stability requirements are found for all pedestrians distributed at the antinode of the mode shape. Although these conditions are unlikely to occur during normal bridge use and can even be unrealistic for large number of pedestrians, they can be considered representative of conditions during controlled crowd loading tests conducted to examine the structural dynamic stability boundaries with the least possible effort (i.e. the lowest number of pedestrians), or to excite a bridge to the levels sufficient to obtain meaningful data for calibration of FE models. Uniform and random distribution of pedestrians on the bridge yield the same expected damping demand at $D_{50,uni} = D_{50,rand}$. However, $D_{95,rand}$ is higher than $D_{95,uni}$ due to the higher variance.

The lateral dynamic stability requirements expressed in terms of D are generally much higher for the second lateral mode of the CSB. This agrees with the results from measurements on the CSB in 2003 [10] during which the instability of the second lateral mode was more pronounced under the action of a crowd having average density up to 1.1 people/m^2 corresponding to 488 pedestrians confined to walking within two narrow footways. Furthermore, a more demanding bridge damping provision is required to meet 95% confidence limit in D for the second lateral mode. This is due to $-\tilde{\mu}_{\Delta C}$ and $\tilde{\sigma}_{\Delta C}$ being generally higher for smaller natural frequencies, f_n, as can be seen in Figure 10.

The results from numerical simulations of CSB response under the action of pedestrians generally corroborate

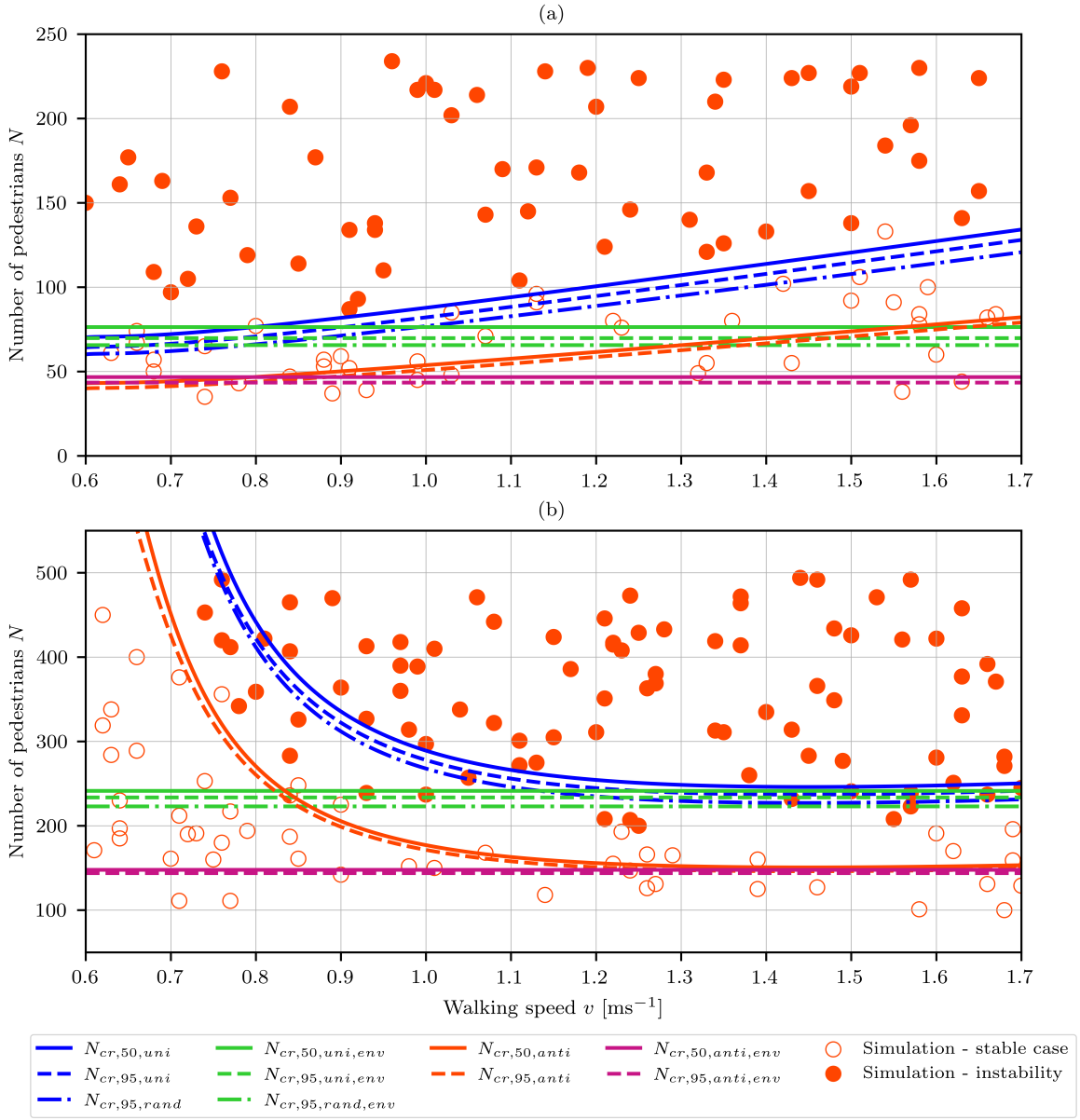

Figure 15: Stability boundaries expressed in terms of the critical number of pedestrians, N_{cr}, relative to the walking speed of pedestrians for the (a) second and (b) third lateral mode of the CSB based on the analytical solutions of $-\tilde{\mu}_{\Delta C}$ and $\tilde{\sigma}_{\Delta C}$, their piecewise-linear envelopes, and numerical simulations of the CSB response.

the results obtained from the stability criteria. It can be seen in Figure 15 that instability occurs for most – but not all, N above the most lenient N_{cr}. This is expected, since the proposed stability criteria are expressed in a probabilistic sense, making allowance for confidence limits. The results for the third lateral mode, shown in Figure 15 (b), are less conservative then those for the second lateral mode, shown in Figure 15 (a), because there are more unstable cases falling below N_{cr} corresponding to the most lenient stability requirements. Closer inspection of this result revealed that the main reason for this is the condition adopted to identify instability, relying on vibration amplitude only, and a finite simulation period adopted to make the best use of available computational resources. The pedestrian force components other than that at the bridge vibration frequency can add or extract energy to/from the bridge depending on the instantaneous phase difference between the pedestrian and bridge motion, causing short-term variations in vibration amplitude. This can lead to spurious identification of instability. Furthermore, for some simulations – typically close to the stability boundaries, the vibration amplitude evolves very slowly, leading to the adopted instability

threshold at 10 mm being reached after 10 minutes of the bridge response build-up. This can lead to spurious identification of stability.

3.5.2 Squibb Park Bridge

The Squibb Park Bridge (SPB) is located on the revitalised waterfront along the East River near the Brooklyn Bridge in the USA. It was opened in 2013 and demolished in 2019 due to the excessive dynamic response under pedestrian loading, after a failed retrofitting attempt. The drama that unfolded is perhaps best captured by the words of Eric Landau, president of the Brooklyn Bridge Park Corporation (BBPP) managing the SPB site: "*(...) you would certainly never hope you'd have to replace something not only that you just built, but that you just fixed.*" [67]. The SPB superstructure was almost completely rebuilt in 2020.

Figure 16: The original SPB inaugurated in 2013, located near the Brooklyn Bridge in the USA. Source: flickr.com; left: gigi_nyc (17/11/2013), right: Dave Pinter (8/4/2013); CC BY-NC-ND 2.0.

The original SPB, shown in Figure 16, consisted of four noncolinear rectilinear sections with a total length of approximately 137 m resting on reinforced concrete pillars via multi-arm supports. The load-bearing elements of the two central spans, each about 37 m long, were space trusses supported through saddles enabling slight slip displacements by four tendons made of galvanised steel stretching underneath the deck. The tendons were led in pairs with the separation reducing from the pillars towards midspan. The trusses' height increased towards midspan in line with the distribution of bending moments for a simply-supported structural arrangement. The wooden trusses, deck and railing posts were made from robinia pseudoacacia. The fasteners and deviators were made of steel brackets, caps and plates, while steel mesh was used to fill the balustrade. The chosen structural solution ensured unobstructed views of the park and, in the longer perspective, of Lower Manhattan, while the choice of materials and lightweight construction were to evoke the experience of walking among the treetops among which the SPB was set. A consequence of the adopted structural solution and the choice of materials was high susceptibility of the SPB to pedestrian-induced vibrations. The initial reports on the dynamic behaviour of the SPB are inconclusive as to the nature of the dynamic response, although most sources quote bounciness [68] and some other quote sway [69], implying the SPB predominantly vibrated in the vertical or lateral direction, respectively. To verify these prepositions, the video footage obtained from [70], taken during a period of instability observed approximately three months after the original SPB opening, was analysed in [66]. The same video is re-analysed herein, but this time applying an image stabilisation procedure to remove the camera motion components prior to the application of optical-flow motion tracking algorithm. The displacement of a point at the midspan of the deck, close to the outermost location in the transverse cross section, was calculated in two orthogonal directions as shown in Figure 17.

The response of the SPB during instability period is shown in Figure 18 (a) in terms of the time histories of displacement filtered with 4th order bandpass Butterworth filter with cut-off frequencies at 0.7 Hz and 1 Hz, and in Figure 18 (b) in terms of the magnitude of fast Fourier transform (FFT) of the displacement. It can

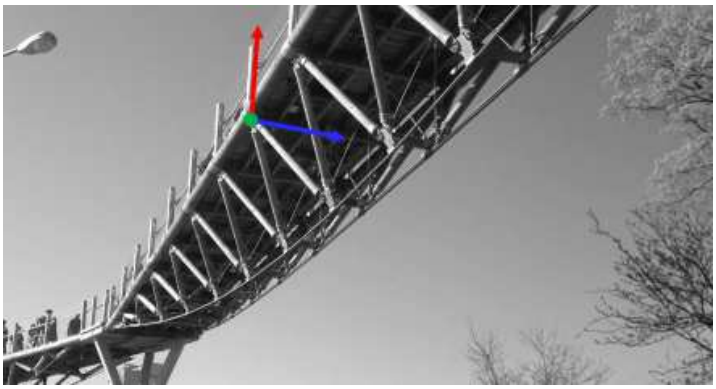

Figure 17: A snapshot from a video showing the dynamic behaviour of the SPB during instability period [70], stabilised prior to the application of motion tracking algorithm to remove camera motion, with the point of measurement of displacement in two orthogonal directions – lateral and vertical.

be seen that the SPB responded predominantly in the lateral direction. The dominant harmonic components occur at a frequency of approximately 0.84 Hz. It can be assumed that this frequency corresponds to one of the modal frequencies of the considered span. During the vibration cycle corresponding to this frequency, the maximum positive displacement in the lateral axis of the bridge occurs simultaneously with the maximum positive displacement in the vertical axis, according to the coordinate system for the measurement point shown in Figure 17.

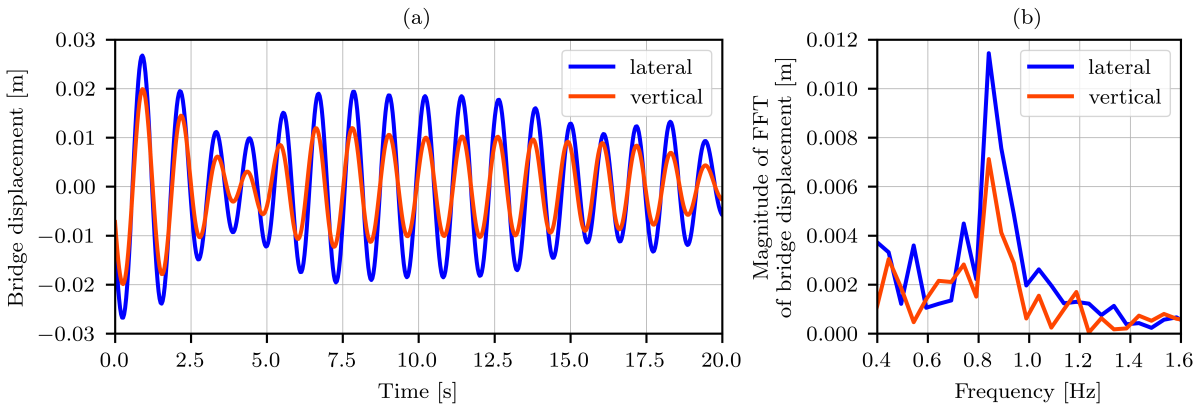

Figure 18: Response of the SPB during instability period in terms of (a) time history of displacement and (b) magnitude of FFT of signals presented in (a) from the measurement point indicated in Figure 17.

To verify this assessment, a finite element (FE) model of the same span of the SPB was built in SOFiSTiK 2022, as shown in Figure 19. The top chord of the truss, cross bracing, lower struts and floor beams transferring the load from the deck to the truss were modelled with beam elements. The deck itself was modelled with shell elements with zero stiffness in the direction of the planks. The bottom chord of the truss was modelled with cable elements. The geometry of the structure and its materials' properties were based on information provided in [71]. The main mode of the span at 0.95 Hz, obtained from the FE model, was characterised by torsional motion with a strong lateral translational component, thus qualitatively confirming the results obtained from the video footage. The modal mass for this mode obtained from the FE model was 9400 kg.

The approach to simulations of the dynamic behaviour of the SPB under the action of pedestrians according to Eqs. 39 and 40 was different to that adopted for the CSB. This is due to the relatively low modal mass of the considered mode hence high sensitivity of m_r – which needs to be updated during the iterative process of finding N_{cr} – to the number of pedestrians on the bridge, N. The simulations commenced with $N = 1$, and

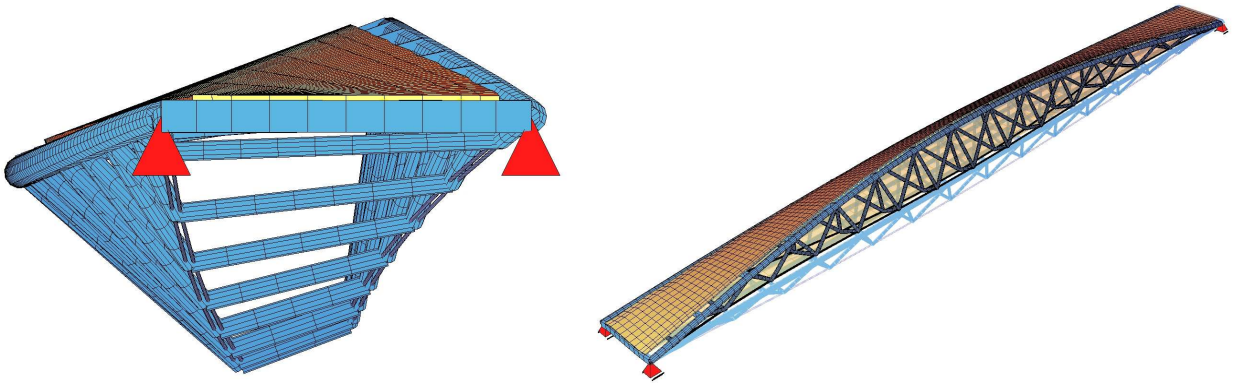

Figure 19: The dominant mode of one of the main spans of the SPB based on the finite element model generated in SOFiSTiK.

continued with unitary increase until $N = N_{cr}$, as defined in Eq. 41. Due to the unavailability of empirical data, the damping ratio of 1.5% was adopted based on the results reported for a similar footbridge [72].

The distribution of results for the SPB in terms of the pedestrian Scruton number, D, presented in Figure 20 is similar to that for the third lateral mode of the CSB presented in Figure 14 (b). However, the confidence limits are generally much wider, which is related to a higher variance in $-\tilde{\mu}_{\Delta C}$ associated with the lower N_{cr}. The most detrimental effect to the structural stability occurs for pedestrians walking at normal and high speeds. As in the case of the CSB, for all considered pedestrian distributions, the results based on piecewise-linear envelopes, denoted with the subscript *env* on the plots, are invariant with respect to the walking speed, v. These results are almost always conservative relative to the corresponding results obtained from the analytical solutions of $-\tilde{\mu}_{\Delta C}$ and $\tilde{\sigma}_{\Delta C}$.

The results of analysis of the critical number of pedestrians, N_{cr}, are presented in Figure 21. It can be said with 95% confidence that lateral instability will occur for 18 randomly distributed pedestrians on the SPB walking at the slowest considered speeds. However, as few as 4 pedestrians are sufficient to drive the bridge to instability if they happen to walk at normal or high speeds. The results from simulations generally support these findings. Good correspondence of results is also found for the piecewise-linear envelopes. Taken together, the presented results suggest extremely high susceptibility of the SPB to the excessive lateral dynamic response under the action of walking pedestrians. Indeed, this can also be deducted from the inspection of the analysed video footage where the SPB seems to be excessively excited by relatively few pedestrians [70]. Considering each of the main spans of the SPB could accommodate dozens of freely walking pedestrians at any given time, it should not be surprising that the original structure remained opened for less than 18 months after inauguration and, ultimately, had to be replaced.

4 Conclusions

Probabilistic criteria for lateral dynamic stability of structures under the loading from walking pedestrians were derived in this study based on outputs from the generalised inverted pendulum pedestrian model (IPM). This required statistical models of the anthropometric parameters defining the generalised IPM to be first determined for the considered population of pedestrians. A methodology for carrying out this task was proposed and demonstrated to provide data of sufficient quality. A methodology was also proposed for identifying an excessive lateral separation between the contralateral foot placements within the analytical solutions of the generalised IPM. This allowed spurious outputs from the generalised IPM to be avoided.

Having established the parameters defining the generalised IPM for a given pedestrian population, the pedestrians-induced self-excited forces were defined for a range of pedestrian walking speeds in terms of the

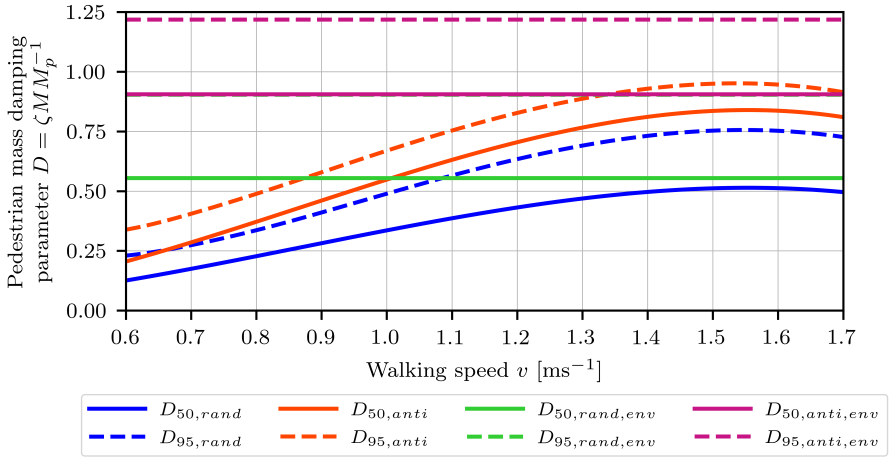

Figure 20: Pedestrian Scruton number, D, relative to the walking speed of pedestrians for the SPB based on the analytical solutions of $-\tilde{\mu}_{\Delta C}$ and $\tilde{\sigma}_{\Delta C}$, and their piecewise-linear envelopes.

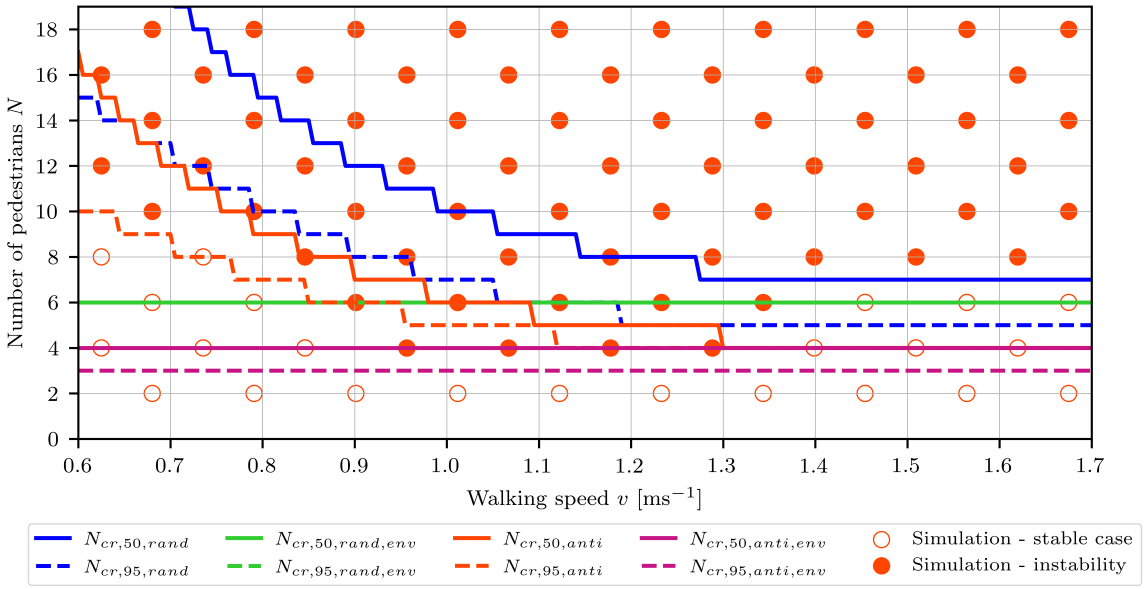

Figure 21: Stability boundaries expressed in terms of the critical number of pedestrians, N_{cr}, relative to the walking speed of pedestrians for the SPB based on the analytical solutions of $-\tilde{\mu}_{\Delta C}$ and $\tilde{\sigma}_{\Delta C}$, their piecewise-linear envelopes, and numerical simulations of the SPB response.

mean equivalent added damping and the corresponding standard deviation, and the mean equivalent added mass. The extreme structural vibration frequency shifts were then determined based on the added mass effect, taking into account the pedestrians-to-structure mass ratio. They were used to find the critical mean equivalent added damping over all considered walking speeds for each natural frequency up to 2 Hz, together with the corresponding standard deviation. An algorithm was then developed to generate piecewise-linear envelopes of these parameters. This step served to simplify their definition, thus making the proposed probabilistic criteria suitable for the inclusion in codified design guidelines. The probabilistic stability conditions were defined in terms of the pedestrian Scruton number, which is a dimensionless mass-damping parameter, and the critical number of pedestrians. Three types of pedestrian distribution on the structure were considered, namely the uniform distribution, random distribution, and all pedestrians distributed at the antinode of the mode shape.

A validation study was carried out using two bridges prone to pedestrian-induced lateral dynamic instability, namely the Clifton Suspension Bridge (CSB) in the UK and the Squibb Park Bridge (SPB) in the USA. The latter case was studied in more detail as it is relatively little known in the structural engineering community. A forensic investigation was therefore conducted to identify the causes of the excessive dynamic behaviour of the SPB, based on the analysis of video footage taken shortly after its opening, and the outputs of a purpose-built finite element model. Good agreement was found between the stability boundaries derived from the critical mean added damping obtained from the generalised IPM and those obtained from numerical simulations of the dynamic response of these two bridges to pedestrian loading, taking into account all pedestrian force components. The stability boundaries obtained from the piecewise linear envelopes of the critical mean equivalent added damping and its standard deviation were shown to capture the most detrimental loading conditions, taking into account the effect of walking speed, whilst not being overly conservative.

The proposed probabilistic stability criteria provide a powerful tool for the design of structures, particularly bridges, against pedestrian-induced lateral instability. They are based on a fundamental model of pedestrian gait for walking on a laterally-oscillating structure calibrated against empirical data, are traceable since they are derived from the closed-form long term solutions of the generalised IPM, and can be easily defined for any population of pedestrians according to the proposed algorithm. They take into account the intensity of the load, the influence of the mode shape and the distribution of pedestrians. They therefore allow different loading conditions to be distinguished and evaluated, enabling the designer to make informed choices, balancing the risk of structural instability against the considered structural solution. Despite their obvious power, they are also easy to apply, as they use the familiar concept of the Scruton number – an index originally used to capture the effects of wind-structure interaction. They can even be expressed in a more intuitive way in terms of the critical number of pedestrians on the bridge.

The main remaining challenge is for the proposed probabilistic stability criteria to find their way beyond the academic discourse. Cases of laterally unstable bridges are regularly reported in the media. Many of these bridges require costly retrofitting solutions, leading to legal disputes over liability, as exemplified herein by the case of the SPB. This can damage the reputation of their designers and lead to high social costs associated with the closure of these structures. This could be avoided, or at least reduced, if appropriate design provisions were included in the national or international structural design standards.

Acknowledgements

This paper is dedicated to the memory of Prof. John H.G. Macdonald from the University of Bristol, UK, who passed away prematurely in March 2022. John introduced the biomechanically-inspired inverted pendulum pedestrian model to the field of structural engineering in 2009 [1]. M. Bocian and B. Czaplewski were supported by the Polish National Agency for Academic Exchange (NAWA) under the Polish Returns programme grant number PPN/PPO/2019/1/00036.

Data availability

The data that support the findings of this study are available from the corresponding author upon request.

References

[1] J. Macdonald, "Lateral excitation of bridges by balancing pedestrians," *Proceedings of the Royal Society of London A: Mathematical, Physical and Engineering Sciences*, vol. 465, pp. 1055–1073, 2009.

[2] B. Czaplewski, M. Bocian, and J. Macdonald, "Calibration of inverted pendulum pedestrian model for laterally oscillating bridges based on stepping behaviour," *Journal of Sound and Vibration*, no. 118141, 2023.

[3] B. Czaplewski and M. Bocian, "Long-term solutions to calibrated and generalised Macdonald's model for pedestrian-induced lateral forces," *Journal of Sound and Vibration*, no. 118494, 2024.

[4] A. McRobie, "Long-term solutions to Macdonald's model for pedestrian-induced lateral forces," *Journal of Sound and Vibration*, vol. 332, pp. 2846–2855, 2013.

[5] M. Bocian, J. Macdonald, and J. Burn, "Probabilistic criteria for lateral dynamic stability of bridges under crowd loading," *Computers & Structures*, vol. 136, pp. 108–119, 2014.

[6] P. Dallard, A. Fitzpatrick, A. Flint, S. Le Bourva, A. Low, R. Ridsdill Smith, and M. Willford, "The London Millennium Footbridge," *The Structural Engineer*, vol. 79, no. 22, pp. 17–21, 2001.

[7] Y. Fujino, B. Pacheco, S. Nakamura, and P. Warnitchai, "Synchronization of human walking observed during lateral vibration of a congested pedestrian bridge," *Earthquake Engineering & Structural Dynamics*, vol. 22/9, pp. 741–758, 1993.

[8] S. Nakamura, "Field measurements of lateral vibration on a pedestrian suspension bridge," *The Structural Engineer*, vol. 81, pp. 22–26, 22 2003.

[9] J. Brownjohn, P. Fok, M. Roche, and P. Omenzetter, "Long span steel pedestrian bridge at Singapore Changi Airport — Part 2: Crowd loading tests and vibration mitigation measures," *The Structural Engineer*, vol. 82, no. 16, pp. 21–27, 2004.

[10] J. Macdonald, "Pedestrian-induced vibrations of the Clifton Suspension Bridge," *Proceedings of the Institution of Civil Engineers – Bridge Engineering*, vol. 161/2, pp. 69–77, 2008.

[11] E. Caetano, Á. Cunha, F. Magalhães, and C. Moutinho, "Studies for controlling human-induced vibration of the Pedro e Inês Footbridge, Portugal. Part 1: Assessment of dynamic behaviour," *Engineering Structures*, vol. 32, no. 4, pp. 1069–1081, 2010.

[12] R. White, N. Alexander, J. Macdonald, and M. Bocian, "Characterisation of crowd lateral dynamic forcing from full-scale measurements on the Clifton Suspension Bridge," *Structures*, vol. 24, pp. 415–425, 2020.

[13] R. Cuevas, J. Jiménez-Alonso, F. Martínez, and I. Díaz, "Assessment of the lateral vibration serviceability limit state of slender footbridges including the postlock-in behaviour," *Applied Sciences*, vol. 10, p. 967, 2020.

[14] A. McRobie and G. Morgenthal, "Risk management for pedestrian-induced dynamics of footbridges," in *Proceedings of the 1st International Conference Footbridge, Paris, France, 20–22 November*, 2002.

[15] A. Pizzimenti and F. Ricciardelli, "Experimental evaluation of the dynamic lateral loading of footbridges by walking pedestrians," *Proceedings of Eurodyn 2005 - 6th International Conference on Structural Dynamics, Paris, France*, 2005.

[16] E. Ingólfsson, C. Georgakis, F. Ricciardelli, and J. Jönsson, "Experimental identification of pedestrian-induced forces on footbridges," *Journal of Sound and Vibration*, vol. 330, no. 6, pp. 1265–1284, 2011.

[17] S. Carroll, J. Owen, and M. Hussein, "Experimental identification of the lateral human-structure interaction mechanism and assessment of the inverted-pendulum biomechanical model," *Journal of Sound and Vibration*, vol. 333, pp. 5865–5884, 2014.

[18] M. Bocian, J. Macdonald, J. Burn, and J. Brownjohn, "Experimental identification of the behaviour of and lateral forces from freely-walking pedestrians on laterally oscillating structures in a virtual reality environment," *Engineering Structures*, vol. 105, pp. 62–76, 2015.

[19] M. Bocian, J. Burn, J. Macdonald, and J. Brownjohn, "From phase drift to synchronisation – pedestrian stepping behaviour on laterally oscillating structures and consequences for dynamic stability," *Journal of Sound and Vibration*, vol. 392, pp. 382–399, 2017.

[20] D. Claff, M. Williams, and A. Blakeborough, "The kinematics and kinetics of pedestrians on a laterally swaying footbridge," *Journal of Sound and Vibration*, vol. 407, pp. 286–308, 2017.

[21] M. Bocian, H. Wdowicka, J. Burn, and J. Macdonald, "Determinants of pedestrian mediolateral foot placement in walking on laterally-scillating structures and their consequences for structural stability," *Mechanical Systems and Signal Processing*, vol. 222, no. 111793, 2025.

[22] B. Castillo, J. Marulanda, and P. Thomson, "Experimental evaluation of pedestrian-induced multiaxial gait loads on footbridges: Effects of the structure-to-human interaction by lateral vibrating platforms," *Sensors*, vol. 24, no. 2517, 2024.

[23] T. Roberts, "Lateral pedestrian excitation of footbridges," *Journal of Bridge Engineering*, vol. 10, no. 1, pp. 107–112, 2005.

[24] A. Blekherman, "Swaying of pedestrian bridges," *Journal of Bridge Engineering*, vol. 10, no. 2, pp. 142–150, 2005.

[25] G. Piccardo and F. Tubino, "Parametric resonance of flexible footbridges under crowd-induced lateral excitation," *Journal of Sound and Vibration*, vol. 311, no. 1-2, pp. 353–371, 2008.

[26] T. Morbiato, R. Vitaliani, and A. Saetta, "Numerical analysis of a synchronization phenomenon: Pedestrian–structure interaction," *Computers & Structures*, vol. 89, no. 17–18, pp. 1649–1663, 2011.

[27] V. Racic and J. Brownjohn, "Mathematical modelling of random narrow band lateral excitation of footbridges due to pedestrians walking," *Computers & Structures*, vol. 90-91, pp. 116–130, 2012.

[28] A. Erlicher, P. Trovato, and A. Argoul, "A modified hybrid van der pol/rayleigh model for the lateral pedestrian force on a periodically moving floor," *Mechanical Systems and Signal Processing*, vol. 41, pp. 485–501, 2013.

[29] J. Qin, S. Law, Q. Yang, and N. Yang, "Pedestrian-bridge dynamic interaction, including human participation," *Journal of Sound and Vibration*, vol. 332, pp. 1107–1124, 2013.

[30] G. Goldsztein, "Lateral oscillations of the center of mass of bipeds as they walk. Inverted pendulum model with two degrees of freedom," *AIP Advances*, vol. 5, p. 107 208, 2015.

[31] I. Belykh, R. Jeter, and V. Belykh, "Foot force models of crowd dynamics on a wobbly bridge," *Science Advances*, vol. 3, no. e1701512, 2017.

[32] V. Joshi and M. Srinivasan, "Walking crowds on a shaky surface: Stable walkers discover Millennium Bridge oscillations with and without pedestrian synchrony," *Biology Letters*, vol. 14, p. 20 180 564, 2018.

[33] Research Fund for Coal & Steel, *Advanced load models for synchronous pedestrian excitation and optimised design guidelines for steel bridges(SYNPEX)*, 2008.

[34] Research Fund for Coal & Steel, *Human induced vibrations of steel structures – Design of footbridges (HIVOSS)*, 2008.

[35] *UK National Annex to Eurocode 1: Actions on structures – Part 2: Traffic loads on bridges (NA+A1:2020 to BS EN 1991-2-2003)*, London, United Kingdom: British Standard Institution, 2003.

[36] C. Barker, "Some observations on the nature of the mechanism that drives the self-excited lateral response of footbridges," in *Proceedings of the 1st International Conference Footbridge, Paris, France, 20–22 November*, 2002.

[37] S. Strogatz, D. Abrams, A. McRobie, B. Eckhardt, and E. Ott, "Crowd synchrony on the Millennium Bridge," *Nature*, vol. 438, no. 7064, pp. 43–44, 2005.

[38] I. Belykh, M. Bocian, A. Champneys, K. Daley, R. Jeter, J. Macdonald, and A. McRobie, "Emergence of the London Millennium Bridge instability without synchronisation," *Nature Communications*, vol. 12, no. 7223, 2021.

[39] P. Pennington, "Auckland Harbour Bridge wobbles when crowds walk on it, documents show," *The New Zealand Herald*, 2023. [Online]. Available: `https://www.nzherald.co.nz/nz/auckland-harbour-bridge-trembles-when-crowds-walk-on-it-documents-show/CLLF3O4DIVBFVCQVSALP3S5JLA/`.

[40] *Eurocode. Basis of structural design (BS EN 1990:2002+A1:2005)*, London, United Kingdom: British Standards Institution, 2002.

[41] U.S. Department of Transportation, *Service life design reference guide*, Federal Highway Agency, USA, 2022.

[42] GBD 2021 Adult BMI Collaborators, "Global, regional, and national prevalance of adult overweight and obesity, 1990–2021, with forecasts to 2050: A forecasting study for the Global Burden of Disease Study 2021," *The Lancet*, vol. Preprint, 2025.

[43] A. Hof, M. Gazendam, and W. Sinke, "The condition for dynamic stability," *Journal of Biomechanics*, vol. 38, no. 1, pp. 1–8, 2005.

[44] M. Bocian, J. Macdonald, and J. Burn, "Modelling of self-excited vertical forces on structures due to walking pedestrians," *Proceedings of Eurodyn 20011 - 8th International Conference on Structural Dynamics, Leuven, Belgium*, 2011.

[45] M. Bocian, J. Macdonald, and J. Burn, "Biomechanically inspired modelling of pedestrian-induced vertical self-excited forces," *Journal of Bridge Engineering*, vol. 18, no. 12, pp. 1336–1346, 2013.

[46] J. Nessler, S. Heredia, J. Bélair, and J. Milton, "Walking on a vertically oscillating treadmill: Phase synchronization and gait kinematics," *PLoS ONE*, vol. 12, no. 1, e0169924, 2017.

[47] A. McRobie, G. Morgenthal, D. Abrams, and J. Predergast, "Parallels between wind and crowd loading of bridges," *Philosophical Transactions of the Royal Society A*, vol. 371, p. 20 120 430, 2013.

[48] B. Jia, Y. Chen, and X. Yu, "Hybrid model for pedestrian-induced lateral vibrations of footbridge based on pedestrian phase evolution and inverted pendulum model: Simulation and validation," *Journal of Bridge Engineering*, vol. 29, no. 8, 2024.

[49] H. Yang, Z. Wang, B. Wu, and Y. Bao, "Investigation of 3D bipedal spring-loaded inverted pendulum human walking model on laterally vibrating surfaces in the case of phase drift, phase pulling, and synchronisation," *International Journal of Structural Stability and Dynamics*, no. 2550220, 2025.

[50] E. Ingólfsson and C. Georgakis, "A stochastic load model for pedestrian-induced lateral forces on footbridges," *Engineering Structures*, vol. 33, pp. 3454–3470, 2011.

[51] F. Ricciardelli and C. Demartino, "Design of footbridges against pedestrian-induced vibrations," *Journal of Bridge Engineering*, vol. 21, p. C4015003, 8 2016.

[52] M. Bocian, J. Macdonald, and J. Burn, "Biomechanically inspired modelling of pedestrian-induced forces on laterally oscillating structures," *Journal of Sound and Vibration*, vol. 331, no. 16, pp. 3914–3929, 2012.

[53] D. Newland, "Pedestrian excitation of bridges," *Proceedings of the Institution of Mechanical Engineers Part C – Journal of Mechanical Engineering Science*, vol. 218, pp. 477–492, 2004.

[54] R. Scanlan and J. Tomko, "Airfoil and bridge flutter derivatives," *Journal of the Engineering Mechanics Division*, vol. 97, no. 6, pp. 1717–1737, 1971.

[55] N. Nikitas, J. Macdonald, and J. Jakobsen, "Identification of flutter derivatives from full-scale ambient vibration measurements of the clifton suspension bridge," *Wind and Structures*, vol. 14, no. 3, pp. 1226–6116, 2011.

[56] E. Jarosz, "Dane antropometryczne populacji osób dorosłych wybranych krajów Unii Europejskiej i Polski dla potrzeb projektowania (Anthropometric data for adults of the selected coutries of the European Union and Poland for the design purposes)," *Instytut Wzornictwa Przemysłowego, Prace i Materiały*, no. 6, 2003.

[57] C. Gordon, C. Blackwell, B. Bradtmiller, J. Parham, P. Barrientos, S. Paquette, B. Corner, J. Carson, J. Venezia, B. Rockwell, M. Mucher, and S. Kristensen, "2012 anthropometric survey of U.S. Army personnel: Methods and summary statistics," *U.S. Army Natick Soldier Research, Development and Engineering Center*, no. NATICK/TR-15/007, 2014.

[58] International Organization for Standardization, *ISO 7250-1:2017: Basic human body measurements for technological design - Part 1: Body measurement definitions and landmarks*, Switzerland, 2017.

[59] C. L. Ogden, C. D. Fryar, M. D. Carroll, and J. Afful, "Anthropometric reference data for children and adults: United states, 2015–2018," National Center for Health Statistics, 159, 2021. [Online]. Available: `https://www.cdc.gov/nchs/data/nhsr/nhsr159-508.pdf`.

[60] World Health Organization. "Mean body mass index trends among adults, age-standardized (kg/m²). Estiamtes by country. "[Online]. Available: https://apps.who.int/gho/data/node.main.A904?lang=en.

[61] K. Zatońska, L. Waszkiewicz, and M. Bolanowski, "Samoocena stopnia otyłości kobiet i mężczyzn zamiszkałych na Dolnym Śląsku (Obesity self-assessment by women and men living in Lower Silesia)," *Endokrynologia, Otyłość i Zaburzenia Przemiany Materii*, vol. 2, no. 1, pp. 12–17, 2006.

[62] National Health Service (NHS), "Health Survey for England – 2008 trend tables," 2009. [Online]. Available: https://digital.nhs.uk/data-and-information/publications/statistical/health-survey-for-england/health-survey-for-england-2008-trend-tables.

[63] National Center for Health Statistics, "Anthropometric reference data for children and adults: United States, 2007–2010," U.S. Department of Health, Human Services, Centers for Disease Control, and Prevention, Oct. 2012. [Online]. Available: https://www.cdc.gov/nchs/data/series/sr_11/sr11_252.pdf.

[64] S. Wilkinson and J. Knapton, "Analysis and solution to human-induced lateral vibrations on a historic footbridge," *Journal of Bridge Engineering*, vol. 11, pp. 4–12, 1 2006.

[65] G. Dean, "An analysis of the energy expenditure in level and grade walking," *Ergonomics*, no. 8, pp. 31–47, 1965.

[66] M. Bocian and B. Czaplewski, "Do trzech razy sztuka – niestabilność dynamiczna mostu dla pieszych w Squibb Park przy Moście Brooklińskim (Third time lucky – dynamic instability of the Squibb Park Bridge near the Brooklyn Bridge)," *Inżynieria i Budownictwo*, vol. 78/1-2, pp. 58–61, 2021.

[67] A. Plitt, "Brooklyn Bridge Park will replace problem-plagued Squibb Bridge," *Curbed NY*, 2018. [Online]. Available: https://ny.curbed.com/2018/12/4/18125867/brooklyn-bridge-park-squibb-park-construction.

[68] A. Cho, "Brooklyn footbridge reopens after three-year closure," *Engineering News Records*, 2017. [Online]. Available: https://www.enr.com/articles/41898-brooklyn-footbridge-reopens-after-three-year-closure.

[69] L. Foderaro, "Park calls upon a new firm to steady its swinging bridge," *The New York Times*, 2016. [Online]. Available: https://www.nytimes.com/2016/01/28/nyregion/new-engineering-firm-called-upon-to-fix-swaying-squibb-park-bridge.html.

[70] M. Carr. "Brooklyn's Squibb Park Bridge," Accessed: May 7, 2013. [Online]. Available: https://www.youtube.com/watch?v=vXu2dzBMUDw.

[71] R. Woodward and T. Zoli, "Two bridges built using black locust wood," *2nd International Conference on Timber Bridges, Las Vegas, USA, 30 September – 2nd October*, 2013.

[72] A. Rönnquist, E. Strømmen, and L. Wollebæk, "Dynamic properties from full scale recordings and FE-modelling of a slender footbridge with flexible connections," *Structural Engineering International*, vol. 18, pp. 421–426, 4 2008.